



# HHS Public Access

Author manuscript

*Mol Cell*. Author manuscript; available in PMC 2020 May 16.

Published in final edited form as:

*Mol Cell*. 2019 May 16; 74(4): 701–712.e9. doi:10.1016/j.molcel.2019.03.006.

## Gain of additional BIRC3 protein functions through 3'UTR-mediated protein complex formation

Shih-Han Lee<sup>1</sup> and Christine Mayr<sup>1,2,\*</sup>

<sup>1</sup>Cancer Biology and Genetics Program, Memorial Sloan Kettering Cancer Center, New York, NY 10065, USA

<sup>2</sup>Lead Contact

### Summary

Alternative 3' untranslated regions (3'UTRs) are widespread but their functional roles are largely unknown. We investigated the function of the long *BIRC3* 3'UTR which is upregulated in leukemia. The 3'UTR does not regulate BIRC3 protein localization or abundance, but is required for CXCR4-mediated B cell migration. We established an experimental pipeline to study the mechanism of regulation and used mass spectrometry to identify BIRC3 protein interactors. In addition to 3'UTR-independent interactors involved in known BIRC3 functions, we detected interactors that bind only to BIRC3 protein encoded from the mRNA with the long 3'UTR. They regulate several functions, including CXCR4 trafficking. We further identified RNA-binding proteins differentially bound to the alternative 3'UTRs and found that cooperative binding of Staufen and HuR mediates 3'UTR-dependent complex formation. We show that the long 3'UTR is required for the formation of specific protein complexes that enable additional functions of BIRC3 protein beyond its 3'UTR-independent functions.

### Graphical Abstract

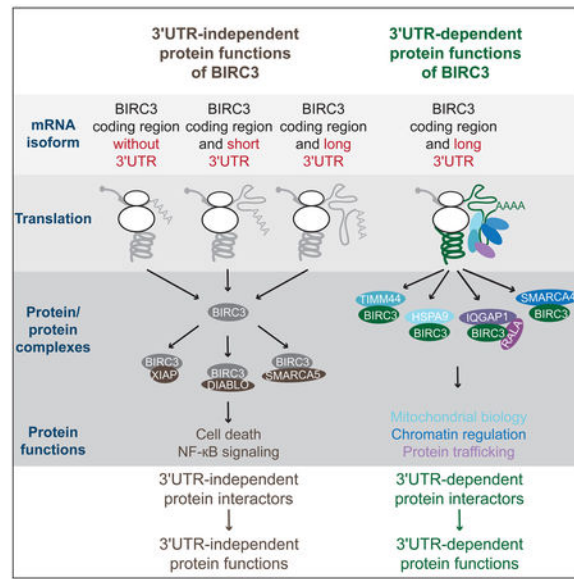
---

\*Correspondence: mayrc@mskcc.org (C.M.), Christine Mayr, Memorial Sloan Kettering Cancer Center, 1275 York Ave, Box 303, New York, NY 10065, Phone: 646-888-3115.

#### Declaration of Interests

The authors declare no competing interests.

**Publisher's Disclaimer:** This is a PDF file of an unedited manuscript that has been accepted for publication. As a service to our customers we are providing this early version of the manuscript. The manuscript will undergo copyediting, typesetting, and review of the resulting proof before it is published in its final form. Please note that during the production process errors may be discovered which could affect the content, and all legal disclaimers that apply to the journal pertain.



### eTOC blurb:

Lee & Mayr show that the E3 ligase BIRC3 has several different functions that are exclusively accomplished by BIRC3 protein encoded from the mRNA transcript containing the long but not the short 3'UTR. 3'UTR-dependent protein functions are caused by BIRC3 protein complexes that require the long 3'UTR for their formation.

### Introduction

Over half of human genes use alternative cleavage and polyadenylation (APA) to generate mRNA transcripts with alternative 3' untranslated regions (3'UTRs) (Lianoglou et al., 2013). APA is a regulated process as the expression ratios of alternative 3'UTR isoforms change in a coordinated manner during many biological processes, including differentiation, immune cell activation or cancer (Sandberg et al., 2008; Mayr and Bartel, 2009; Gruber et al., 2014; Brumbaugh et al., 2018). Initially, when alternative 3'UTRs were discovered to be widespread, it was thought that their major role is the regulation of protein abundance (Sandberg et al., 2008; Mayr and Bartel, 2009). Indeed, many genes that encode short-lived mRNAs, including cytokines, cell cycle regulators or oncogenes use their 3'UTRs to regulate protein abundance (Mayr, 2018). However, several genome-wide studies have observed that generally less than 20% of significant 3'UTR isoform changes are associated with changes in their corresponding mRNA or protein expression levels (Lianoglou et al., 2013; Spies et al., 2013; Gruber et al., 2014; Brumbaugh et al., 2018). Instead, when changes in APA were assessed during diverse biological processes, it was repeatedly observed that genes that changed their mRNA abundance levels largely did not change their 3'UTR isoform expression and vice versa (Lianoglou et al., 2013; Zhang et al., 2016; Jia et al., 2017). Therefore, it is still mostly unclear, how the changes in alternative 3'UTR isoform ratios contribute to biology (Mayr, 2017).

One way to use alternative 3'UTRs for the regulation of biological processes is through 3'UTR-mediated protein-protein interactions (Berkovits and Mayr, 2015; Ma and Mayr, 2018). It was shown that the long 3'UTR of *CD47* increases CD47 plasma membrane localization, thus protecting cells better from phagocytosis by macrophages (Berkovits and Mayr, 2015). The increase in plasma membrane trafficking was caused by the binding of the adaptor SET to CD47. SET transfer from the 3'UTR to the newly synthesized protein occurs in a membraneless organelle that is associated with the endoplasmic reticulum (Ma and Mayr, 2018).

Here, we set out to establish an experimental pipeline to identify 3'UTR-dependent protein interactors and to study the functions of long 3'UTRs. We used *BIRC3* as candidate as its long 3'UTR isoform was significantly upregulated in malignant B cells derived from chronic lymphocytic leukemia (CLL). *BIRC3* encodes an E3 protein ubiquitin ligase that does not contain a transmembrane domain. It is known to regulate cell death and immune functions through negative regulation of the NF- $\kappa$ B pathway (Beug et al., 2012).

Despite upregulation of the long *BIRC3* 3'UTR in CLL, we observed that overall *BIRC3* mRNA and *BIRC3* protein levels were similar between normal and malignant B cells. To study the function of the long 3'UTR, we identified 3'UTR-dependent protein interactors of *BIRC3*. We call *BIRC3* protein encoded from the long *BIRC3* 3'UTR isoform, *BIRC3*-LU, and *BIRC3* protein encoded from the short 3'UTR isoform, *BIRC3*-SU. Both *BIRC3*-SU and *BIRC3*-LU can accomplish 3'UTR-independent functions, such as the cell-intrinsic control of cell death. However, only *BIRC3*-LU has the ability to regulate CXCR4-mediated B cell migration; an event that is crucial for CLL cell survival by enabling the homing of B cells to protective bone marrow niches (Burger et al., 2005). *BIRC3*-LU accomplishes this function through 3'UTR-mediated protein complex assembly involving IQGAP1 and RALA. In addition to regulating protein trafficking, *BIRC3*-LU binds to numerous other 3'UTR-dependent interactors allowing it to perform additional roles. Cooperative binding of RNA-binding proteins throughout the long 3'UTR enables the unique functions of the long 3'UTR by recruiting specific factors that participate in the formation of 3'UTR-dependent protein complexes. This allows *BIRC3* protein to achieve several 3'UTR-dependent functions in addition to its 3'UTR-independent functions.

## Results

### Similar *BIRC3* mRNA level in normal and malignant B cells, but upregulation of the long 3'UTR isoform in CLL

Our goal was to study regulatory functions of 3'UTRs that are independent of protein abundance regulation. We analyzed 3'UTR isoform expression between normal CD5+ B cells from healthy individuals (NB,  $N=4$ ) and CLL patients ( $N=13$ ) (Lee et al., 2018). We observed shortening and lengthening of 3'UTRs, but 66% of mRNA isoforms (412/627) expressed higher levels of longer 3'UTRs in leukemia (Figure S1A, Table S1). *BIRC3* was our top candidate for follow-up experiments as expression of the long 3'UTR was significantly upregulated in all tested CLL samples (Figures 1A, 1B, S1B), but overall *BIRC3* mRNA and protein levels were similar between normal and malignant B cells (Figures 1C, 1D, S1C, S1D).

### Subcellular mRNA and protein localization of GFP-BIRC3-SU and GFP-BIRC3-LU is similar

To test if the alternative 3'UTR isoforms may influence mRNA or protein localization, we generated GFP-BIRC3 fusion constructs either containing the short (631 nucleotides) or long (2,299 nucleotides) *BIRC3* 3'UTRs (Figure 1E). Single molecule RNA-FISH on the transfected constructs did not reveal a difference in mRNA localization caused by the alternative 3'UTRs (Figure 1F). Also, the alternative *BIRC3* 3'UTRs did not influence BIRC3 protein localization (Figure 1G).

### Knock-down of the long BIRC3 3'UTR isoform to study the function of BIRC3-LU in B cells

We next set out to find a phenotype that is caused by BIRC3-LU, but not by BIRC3-SU, and worked with the malignant B cell line Raji as CLL cells cannot be cultivated. Using CRISPR-Cas9, we generated Raji cells that lack BIRC3 protein (BIRC3 knock-out (KO); Figures 2A, S2A). Parental Raji (wild-type, WT) and control (ctrl) KO cells that underwent the KO procedure, but still express BIRC3 protein served as controls (Figure S2B). To study the functions of BIRC3-LU which is BIRC3 protein encoded by the long *BIRC3* 3'UTR isoform, we stably expressed shRNAs that target exclusively the long 3'UTR (LU knock-down (KD), Figure 2A). Northern blots were used to validate the extent of KD (Figure S2C). LU KD cells are expected to only express BIRC3-SU, whereas Raji cells stably expressing a control shRNA (ctrl KD) are expected to express both BIRC3-SU and BIRC3-LU proteins (Figure 2A).

### BIRC3 protein regulates cell death in a 3'UTR-independent manner, but it regulates B cell migration in a 3'UTR-dependent manner

BIRC3 is known as anti-apoptotic protein (Beug et al., 2012). We tested B cell survival in our experimental system after treatment with Fludarabine. As expected, BIRC3 KO cells had fewer surviving cells than ctrl Raji cells (Figure 2B), but loss of BIRC3-LU did not significantly influence B cell survival (Figure 2B). This confirms that BIRC3 has anti-apoptotic activity and this function of BIRC3 protein is 3'UTR-independent.

To identify BIRC3 functions that are specific for BIRC3-LU, we performed additional phenotypic assays. BIRC3 belongs to the family of IAP (inhibitor of apoptosis) proteins and homologues from flies were implicated in the regulation of migration (Geisbrecht and Montell, 2004). This prompted us to test if B cell migration is regulated by mammalian BIRC3. Compared with ctrl cells, the migratory capacity of BIRC3 KO cells was severely impaired (Figure 2C). Strikingly, migration was also impaired in LU KD cells (Figure 2C). As LU KD cells still express BIRC3-SU (Figure S2B), this experiment showed that only BIRC3-LU, but not BIRC3-SU, is required for B cell migration. Taken together, our data indicate that BIRC3 protein has 3'UTR-independent functions, including the control of cell death (Figure 2B), but it also has 3'UTR-dependent functions, such as the regulation of B cell migration (Figure 2C).

### BIRC3-LU regulates surface expression of CXCR4

We next asked how BIRC3-LU regulates B cell migration. The migration assay was performed in the presence of the cytokine CXCL12. CXCR4, the receptor for CXCL12, is expressed on normal and malignant B cells, and is known as an important survival factor in

CLL as it allows CLL cells to migrate to protective bone marrow niches (Burger et al., 2005).

To elucidate how BIRC3-LU regulates CXCR4 expression, we investigated if BIRC3 regulates *CXCR4* mRNA levels. Endogenous CXCR4 mRNA and protein levels were not affected in Raji cells lacking BIRC3 or lacking BIRC3-LU (Figures S2D-I). Instead, compared with ctrl B cells, we observed significantly lower surface expression of CXCR4 in B cells lacking BIRC3 or lacking BIRC3-LU (2D, 2E, S2J, S2K).

These results suggested that BIRC3-LU, but not BIRC3-SU, regulates surface CXCR4 expression. To corroborate this finding, we performed a rescue experiment. We used the BIRC3 KO3 cell line and re-expressed GFP-tagged BIRC3-SU, GFP-BIRC3-LU, or GFP alone. Despite similar protein expression of BIRC3-SU and BIRC3-LU, only the presence of GFP-BIRC3-LU was able to significantly increase surface expression of endogenous CXCR4 (Figures 2F, S2L).

Regulation of surface CXCR4 expression has been widely studied. Binding of the ligand CXCL12 to CXCR4 results in receptor internalization and partial re-expression at the plasma membrane to allow receptor re-sensitization (Grundler et al., 2009; Marchese, 2016). We performed a recycling assay to test if BIRC3-LU regulates CXCR4 receptor trafficking (Figure S2M). Absence of BIRC3-LU did not influence internalization of CXCR4, but it significantly reduced re-expression at the surface after ligand binding (Figure 2G). This suggests that BIRC3-LU regulates the recycling of CXCR4 back to the plasma membrane after receptor activation.

### **Despite similar CXCR4 mRNA levels, surface CXCR4 expression is increased in CLL cells compared to normal B cells**

The relationship between BIRC3-LU and CXCR4 was also true in primary cancer cells derived from patients with CLL. Despite similar *CXCR4* mRNA levels in normal and CLL B cells (Figure 2H), we observed increased surface CXCR4 expression in CLL (Figure 2I). The *BIRC3* gene is located on chromosome 11q, a region that is heterozygously deleted in 15-20% of CLL patients (Rose-Zerilli et al., 2014). Therefore, currently, BIRC3 is regarded as a tumor-suppressor gene in CLL. In our patient cohort, overall *BIRC3* mRNA expression was reduced in samples with 11q deletions, but they still had a relative increase in expression of the long *BIRC3* 3'UTR isoform (Figures S1E, S1F) (Lee et al., 2018). Importantly, even in CLL samples with 11q deletions, surface CXCR4 levels were upregulated and were expressed at comparable levels as in the remaining CLL samples (Figures S1G, S1H). This shows that in primary CLL cells, increased levels of BIRC3-LU correlate with upregulated surface CXCR4 expression. As BIRC3-LU is responsible for surface CXCR4 expression in malignant B cells (Fig. 2F), our results indicate that BIRC3-LU has a cancer-promoting role in CLL (Figure 2J).

### **Identification of 3'UTR-independent and 3'UTR-dependent interaction partners of BIRC3 protein**

As the long *BIRC3* 3'UTR did not regulate BIRC3 protein abundance or localization, we hypothesized that the 3'UTR may facilitate formation of alternative protein complexes.

Through participation in different protein complexes, BIRC3-SU and BIRC3-LU could accomplish different protein functions. To test this hypothesis, we determined the protein interaction partners of BIRC3 using quantitative mass spectrometry (MS; Figure 3A). We expressed GFP-BIRC3-SU and GFP-BIRC3-LU in cells grown in light and heavy SILAC media, respectively. This was followed by co-immunoprecipitation (co-IP) of GFP and analysis of the proteins bound to either GFP-BIRC3-SU or GFP-BIRC3-LU protein. We calculated the log<sub>2</sub>-based enrichment ratio of each protein interaction partner obtained from the heavy versus the light fraction and ranked them (Figure S3A, Table S2). We defined 3'UTR-independent interactors as proteins that bind equally well to BIRC3-SU and BIRC3-LU. They have LU/SU log<sub>2</sub>-enrichment ratios of approximately zero ( $N=520$ , Figures 3B, grey, S3A). In contrast, interaction partners with higher LU/SU ratios are regarded as long 3'UTR-dependent or BIRC3-LU-enriched interactors ( $N=394$ , Figures 3B, dark green, S3A).

### **BIRC3-LU-dependent interactors are involved in mitochondrial biology, chromatin regulation, and protein trafficking**

Gene ontology analysis revealed that the 3'UTR-independent BIRC3 interactors were significantly enriched in factors that participate in ubiquitin-dependent regulation of NF- $\kappa$ B (Figures 3C, S3B). This is consistent with the known function of BIRC3 as E3 ubiquitin ligase involved in NF- $\kappa$ B pathway regulation (Beug et al., 2012). The BIRC3-LU-enriched interactors clustered into three major functional categories and localize to mitochondria, are chromatin regulators, or are involved in protein trafficking. These functions were largely not found among the 3'UTR-independent interactors (Figures 3C, S3B).

We then validated the candidates using GFP co-IP followed by western blot analysis. We were able to validate 8/10 candidates which indicates a high validation rate (80%). Among the validated BIRC3 interactors were two known interaction partners (DIABLO, XIAP) as well as six previously unknown interactors (Figures 3D, S3C). 5/6 of the previously unknown interactors were BIRC3-LU-enriched and included the chromatin regulator SMARCA4, the mitochondria-localized chaperone HSPA9 and the mitochondrial inner membrane translocase TIMM44. They also consisted of factors involved in protein trafficking, including the IQ motif containing GTPase activating protein 1 (IQGAP1) and the Ras GTPase RALA (Figure 3D). Taken together, the validated interactors of BIRC3 confirm the different functional gene classes obtained by gene ontology analysis.

We were surprised to find a large number of interactors. However, BIRC3 protein has six protein interaction domains (three BIR domains, a UBA, CARD, and RING domain (Figure S3D) (Beug et al., 2012). This may give BIRC3 ample opportunity to bind proteins in a 3'UTR-independent or 3'UTR-dependent manner.

### **Mechanism of 3'UTR-dependent interaction between BIRC3-LU, IQGAP1, and RALA**

As our goal was to elucidate the molecular mechanism of CXCR4 trafficking regulation by BIRC3-LU, we focused on the interaction between known trafficking factors with BIRC3-LU. IQGAP1 was previously shown to regulate CXCR4 recycling in T cells. It is a large protein that provides a scaffold for several signaling pathways but also acts as cytoskeleton-



binding protein with important roles in migration (Bamidele et al., 2015). The Ras GTPase RALA plays crucial roles in the regulation of actin dynamics, migration, and membrane protein trafficking (Neyraud et al., 2012).

Our MS validation results indicated that the long 3'UTR of *BIRC3* is required for the protein-protein interaction between BIRC3 and IQGAP1 or RALA. There are two possible models for 3'UTR-dependent protein complex formation (Figure 4A). In model 1, BIRC3 acts as an RNA-binding protein that only binds to the long, but not the short *BIRC3* 3'UTR. 3'UTR-bound BIRC3 interacts in an RNA-dependent manner either directly with IQGAP1 and RALA or indirectly through other RNA-binding proteins.

To test if BIRC3 is an RNA-binding protein, we performed RNA affinity pull-down experiments. We *in vitro* transcribed and biotinylated the short (*SU*) and long (*LU*) *BIRC3* 3'UTRs and incubated them with cell lysate prepared from Raji cells that endogenously express BIRC3 protein. Using streptavidin beads, we pulled-down proteins bound to the 3'UTRs and found that BIRC3 protein is not an RNA-binding protein as it did not interact with the 3'UTRs (Figures 4B, 4C).

Model 1 predicts that the protein-protein interaction between BIRC3 and IQGAP1/RALA is RNA-dependent and would still occur when a BIRC3 construct lacking the coding region is being used for co-IP as the protein complex assembles on the long *BIRC3* 3'UTR. Whereas we disproved the predictions of model 1 (Figures 4D, S4A, S4B), all observations are consistent with model 2, where the long *BIRC3* 3'UTR recruits IQGAP1 and RALA to the site of BIRC3 protein translation (Figure 4A). We showed that only the long but not the short *BIRC3* 3'UTR is able to assemble the BIRC3/IQGAP1/RALA complex, indicating that the long 3'UTR is required for the establishment of the interaction (Figures S4C, S4D). However, the long 3'UTR was not required for maintaining the complex after its formation, as the addition of RNase A during co-IP did not disassemble previously formed complexes (Figure 4D). As only the long and not the short 3'UTR recruits the interactors, only the protein encoded from the long transcript can establish the 3'UTR-dependent complex.

### Differential binding of RNA-binding proteins to the alternative 3'UTRs of BIRC3

According to our current model (Figure 4A, model 2), IQGAP1 and RALA are recruited by the long *BIRC3* 3'UTR. As the recruited proteins lack RNA-binding domains, we expect them to associate with the 3'UTR through RNA-binding proteins. We set out to identify the RNA-binding proteins that are responsible for the recruitment of IQGAP1 and RALA to BIRC3-LU. We used the *in vitro* transcribed biotinylated 3'UTRs from above (Figure 4B), followed by pull-down of the bound RNA-binding proteins and western blot analysis as read-out. To evaluate binding specificity, we used the antisense sequences of each 3'UTR.

The RNA-binding protein candidates for testing were obtained from the MS experiment (Figure S3A, Table S2). We had found a large number of RNA-binding proteins as potential interactors of BIRC3 in the MS experiment, but we were not able to validate them by western blot analysis as true BIRC3 protein interactors (Figure S5A). This suggests that RNA-binding proteins are not being transferred from the 3'UTR to the newly made protein, but that they are part of the mRNP complex during translation of BIRC3 protein. We chose

RNA-binding proteins that were enriched in the BIRC3-LU sample (Figure S5B) and tested if they interacted better with the long than the short *BIRC3* 3'UTR, when equal numbers of RNA molecules were used for RNA affinity pull-down (Figures 5A, S5C). Out of 14 tested RNA-binding proteins, six were involved in splicing and mRNA processing. Five of them did not bind to the *BIRC3* 3'UTRs and one of them bound rather unspecifically (Figures 5A, see legend, S5C). From the remaining eight RNA-binding proteins, FUS did not bind, but seven of them bound better to the long than the short *BIRC3* 3'UTR (Figure 5A).

As *LU* is approximately three-times longer than *SU*, *LU* is expected to contain three-times more biotinylated nucleotides than *SU* (Figure 4B). To control for the number of biotins in the RNAs used for RNA affinity pull-down, we repeated the experiment and added three- or six-fold more *SU* than *LU* to the cell lysates. Higher amounts of *SU* increased the binding of several RNA-binding proteins to *SU*. However, even after normalization to the number of biotinylated nucleotides, HuR, IGF2BP1, and hnRNPA1 still bound better to *LU* than to *SU* (Figures 5B, S5C).

### **Staufen and HuR are necessary for the recruitment of RALA and IQGAP1 to BIRC3-LU**

In order to identify the RNA-binding proteins that are responsible for the recruitment of IQGAP1 and RALA, we used shRNAs to knock-down specific RNA-binding proteins. We chose the double-stranded RNA-binding protein Staufen homolog 1 (STAU1) as it is a known interactor of IQGAP1 (Villace et al., 2004). The interaction between STAU1 and IQGAP1 was confirmed by us using MS (Table S3). We stably knocked-down STAU1 (Figure S5D) and repeated the GFP co-IP after expression of GFP-BIRC3-SU or GFP-BIRC3-LU. This allowed us to examine if lack of STAU1 influences 3'UTR-dependent protein complex formation between BIRC3-LU and IQGAP1/RALA. KD of STAU1 did not change protein levels of IQGAP1, RALA or BIRC3 (Figure 5C, input panel). However, it abrogated the 3'UTR-mediated binding of IQGAP1 and RALA to BIRC3-LU, indicating that STAU1 is necessary for the recruitment of both BIRC3-LU-specific interactors.

We next tested if the RNA-binding protein HuR was necessary for IQGAP1/RALA recruitment, as HuR bound better to *LU* than to *SU* (Figure 5B). KD of HuR did not affect protein expression levels of STAU1, IQGAP1, RALA or BIRC3 (Figures 5D, input panel, S5E). However, it prevented the 3'UTR-mediated binding of IQGAP1 and RALA to BIRC3-LU (Figure 5D). In contrast, KD of IGF2BP1, another RNA-binding protein that bound better to *LU* than to *SU* did not affect the binding of several 3'UTR-dependent interactors (Figures S5F, S5G). Taken together, these experiments revealed that not all RNA-binding proteins that interact with the long 3'UTR are required for the recruitment of specific BIRC3 interaction partners. These data suggest that different RNA-binding proteins may recruit different groups of interactors. Whereas STAU1 and HuR recruit IQGAP1 and RALA, IGF2BP1 is likely to recruit other interactors of BIRC3-LU (Figure 5E).

We then asked if STAU1 and HuR are sufficient for the recruitment of IQGAP1 and RALA to BIRC3 protein. We used the MS2 system to tether STAU1 and HuR to BIRC3-SU (Figure 5F). MS2-binding sites (MS2) form RNA hairpins that specifically bind the MS2 coat protein (MCP) (Berkovits and Mayr, 2015). We added MS2 to GFP-BIRC3-SU to obtain GFP-BIRC3-MS2-SU.



We further fused either STAU1 or HuR to an mCherry (mC)-tagged MCP (MCP-mC-STAU1, MCP-mC-HuR). Co-expression of all three constructs tethers STAU1 and HuR to the short 3'UTR of *BIRC3* mRNA. We performed GFP co-IP and observed 3'UTR-dependent recruitment of endogenous IQGAP1 and RALA to GFP-BIRC3-MS2-SU in the presence of STAU1 and HuR (Figures 5F, 5H).

These experiments demonstrated that in the context of a cell lysate the RNA-binding proteins STAU1 and HuR are necessary and sufficient for the 3'UTR-mediated binding of IQGAP1 and RALA to BIRC3. Our results further indicate that mere overexpression of STAU1 and HuR without their tethering to the 3'UTR is not sufficient for 3'UTR-dependent protein complex assembly as binding of IQGAP1/RALA was not observed in the SU sample or in the MCP sample (Figure 5F). This demonstrates that 3'UTR tethering of the RNA-binding proteins to the site of translation is required for 3'UTR-dependent protein complex formation.

### **The stoichiometry of 3'UTR-bound HuR and STAU1 is important for the recruitment of IQGAP1 and RALA**

We then tried to identify the binding sites of STAU1 and HuR in the long *BIRC3* 3'UTR that are responsible for the recruitment of IQGAP1 and RALA. STAU1 does not bind to specific motifs, but is known to bind to double-stranded RNA (Sugimoto et al., 2015). In our RNA affinity pull-down assay STAU1 bound to both *BIRC3* 3'UTRs (Figure 5B), whereas HuR bound better to *LU* than to *SU* (Figures 5A, 5B, 5C). The sequence of *LU* that is not present in *SU* contains seven AREs (Figure 5G), which are known binding sites of HuR (Mayr, 2018; Ma and Mayr, 2018). As 5/7 *LU*-unique AREs clustered within a fragment of *LU*, called *LUI*, we tested if this fragment is able to recapitulate the HuR binding pattern observed with full-length *LU*. This experiment showed that despite the presence of five AREs, HuR did not bind to *LUI* (Figures 5A, 5B). In contrast, the five AREs present in *SU* bind to HuR in a concentration-dependent manner (Figures 5A, 5B). These observations indicate that STAU1 and HuR bind to both *LU* and *SU*, especially if *SU* is present at high concentrations.

Importantly, we observed a quantitative difference in HuR binding: HuR binds better than STAU1 to the full-length long 3'UTR than to *SU* or *LUI* alone, indicated by an increased ratio in the western blot signal for HuR compared with STAU1 in the *LUI* lanes of Figures 5B and 5C. This result suggests that HuR binds to several sites located throughout the entire long 3'UTR (including the sequence of *SU*) to achieve proper HuR binding. Despite binding of both STAU1 and HuR to the short 3'UTR, our results from above showed that the short 3'UTR was unable to mediate recruitment of the trafficking factors IQGAP1 and RALA. This suggests that the ratio of bound HuR to STAU1 is important for the BIRC3-LU-specific protein trafficking function (Figure 5H).

Remarkably, our results indicate that in order to achieve a specific function of the long *BIRC3* 3'UTR, exclusive binding of RNA-binding proteins to *LU* is not required. Instead, through cooperative binding to sites located throughout the entire long 3'UTR a proper stoichiometry of the RNA-binding proteins HuR and STAU1 is achieved which is necessary for the recruitment of IQGAP1 and RALA.

### **BIRC3-LU recruits the protein complex consisting of IQGAP1 and RALA to CXCR4 receptor**

As our goal was to investigate how BIRC3-LU regulates CXCR4 recycling, we examined if BIRC3 interacts with CXCR4 receptor. We transfected into HEK293T cells CXCR4 tagged with myc at the C-terminus (CXCR4-myc) and either GFP-BIRC3-SU, GFP-BIRC3-LU or GFP-BIRC3-NU (without 3'UTR, but with a polyadenylation signal) (Figure 6A). Co-IP of CXCR4-myc showed interaction between CXCR4 and BIRC3 protein translated from any of the three constructs, indicating that BIRC3 protein interacts with CXCR4 in a 3'UTR-independent manner (Figure 6B). However, importantly, the interaction of endogenously expressed IQGAP1 and RALA with CXCR4 required the presence of BIRC3-LU (Figures 6B, S6A). This suggested that the protein complex consisting of BIRC3-LU, IQGAP1 and RALA was recruited to CXCR4 upon BIRC3-LU binding (Figure 6C). As BIRC3-SU was not able to bind to IQGAP1 and RALA (Figures 3D, 4D, 5C-F), BIRC3-SU was incapable to deliver IQGAP1 and RALA to CXCR4, when it interacted with CXCR4 (Figures 6B, 6C).

### **IQGAP1 and RALA are required for surface CXCR4 expression and B cell migration**

So far, our data showed that the cytoskeleton-associated factors IQGAP1 and RALA only interact with CXCR4 in the presence of BIRC3-LU. We next tested if the two factors are necessary for surface expression of CXCR4. KD of IQGAP1 or RALA in Raji B cells significantly decreased surface expression of endogenous CXCR4 without affecting total CXCR4 expression and mimicked the effect observed in LU KD cells (Figures 6D, 6E, S6B-E), suggesting that IQGAP1 and RALA regulate CXCR4 trafficking. Moreover, both cytoskeleton-associated factors were necessary for B cell migration and again mimicked the effects of loss of BIRC3-LU protein (Figure 6F). Taken together, these results demonstrated that BIRC3-LU assembles a protein complex containing IQGAP1 and RALA and recruits these factors to CXCR4 to regulate surface levels of the receptor which is required for B cell migration towards the CXCL12 cytokine.

### **BIRC3-LU, IQGAP1, and RALA are required for trafficking of CD27 receptor**

Lastly, we asked if the regulation of trafficking is specific to CXCR4 or if BIRC3-LU may regulate trafficking of additional surface receptors. We used FACS analysis to measure surface expression of various receptors important for B cell biology. We compared the surface expression of CD19, CD27, CD38, and CD47 between ctrl cells and LU KD cells. LU KD did not affect surface expression of CD19, CD38 or CD47 (Figures S7A-C), but it significantly reduced surface expression of CD27 (Figure S7D), a marker for memory B cells. A similar reduction in CD27 surface expression was observed in BIRC3 KO cells as well as after IQGAP1 KD or RALA KD (Figures S7E, 7F). In none of the conditions tested overall CD27 protein levels were affected (Figure S7G), suggesting that BIRC3-LU, through its interaction with IQGAP1 and RALA, regulates trafficking of at least two cell surface receptors that play important roles in B cell biology.

### **Gain of protein functions through 3'UTR-mediated protein complex formation has the potential to be widespread**

Figure 7A summarizes our findings on the 3'UTR-independent as well as 3'UTR-dependent functions of BIRC3. Through 3'UTR-independent interactors, BIRC3 protein regulates NF-

$\kappa$ B signaling and cell death, whereas through 3'UTR-dependent interactors, BIRC3 regulates mitochondrial biology, chromatin, and protein trafficking. Whereas 3'UTR-independent functions can be achieved by BIRC3 protein that was synthesized from any construct that contains the BIRC3 coding region, 3'UTR-dependent functions can only be performed by BIRC3 protein that was translated from the *BIRC3* mRNA with the long 3'UTR (Figure 7A).

We anticipate that BIRC3 is not the only protein that is able to gain additional functions through 3'UTR-dependent protein complex formation. When we compared 3'UTR isoform expression between normal and CLL B cells, we found that a number of mRNAs changed their mRNA abundance levels (Figure 7B, green) as expected. Other mRNAs changed their 3'UTR ratios (Figure 7B, red, blue). Strikingly, in 94% of the observed mRNA changes either 3'UTR ratios or mRNA levels were altered and in only 6% of changes both features were affected (Figure 7B, black). This means that the vast majority of alternative 3'UTR isoform changes between normal and CLL B cells do not alter the corresponding mRNA levels. Instead, it is likely that a sizable fraction of significant 3'UTR isoform changes are associated with changes in protein functions caused by 3'UTR-dependent protein complex formation.

## Discussion

We chose to investigate the role of the long *BIRC3* 3'UTR isoform in CLL cells as it was consistently upregulated in malignant B cells compared with their normal B cell counterparts. This is an unusual feature, because CLL is a heterogenous disease and only very few markers are present in all CLL samples (Sutton and Rosenquist, 2015). Despite a significant *BIRC3* 3'UTR ratio change, the alternative 3'UTRs did not regulate BIRC3 protein localization or abundance. Instead, we show that BIRC3 protein can accomplish unique functions through 3'UTR-dependent protein complex formation. These functions can only be accomplished by the protein encoded from the mRNA with the long *BIRC3* 3'UTR. One of the newly discovered 3'UTR-dependent functions is the regulation of CXCR4-mediated B cell migration which is an important requirement for CLL cell survival *in vivo* (Burger et al., 2005), indicating that BIRC3-LU has a cancer-promoting role in CLL.

### BIRC3-LU has cancer-promoting functions in CLL

Expression of CXCR4 on the surface of B cells mediates homing of cells to protective bone marrow niches, thus, enhancing CLL cell survival (Burger et al., 2005). The cancer-promoting function of BIRC3-LU is in contrast to BIRC3's assumed role as a tumor-suppressor gene in CLL (Rossi et al., 2012). This view emerged because *BIRC3* is part of a region located on chromosome 11q that is heterozygously deleted in 15-20% of CLL patients. In 83% of cases with 11q deletions, BIRC3 is deleted together with 40 other genes (Rose-Zerilli et al., 2014) which reduces overall *BIRC3* mRNA levels by approximately 50%. Despite the reduction in overall *BIRC3* mRNA levels, all our investigated CLL samples overexpressed the long *BIRC3* 3'UTR isoform. This correlated with increased expression of CXCR4 protein on the surface of CLL cells and with B cell migration. Together with the data obtained in a B cell line, this indicates that reduced BIRC3 levels are

still sufficient for trafficking regulation of CXCR4 and suggests that for 3'UTR-dependent protein complexes protein abundance may not be the determining parameter.

### **3'UTR-dependent protein complex formation can change protein functions independently of protein localization**

Many proteins form complexes to accomplish their cellular functions. So far, it has been largely thought that protein interactions are solely based on protein sequence and conformation as they can be accomplished using constructs that lack any 3'UTR regulatory sequences or can be recapitulated *in vitro* using purified proteins (Huttlin et al., 2017). We call these interactors and their mediated functions 3'UTR-independent. The formation of these complexes often increases with high abundance of the interactors. In contrast, for 3'UTR-dependent protein complex formation, the protein sequence is necessary but not sufficient as the establishment of the protein-protein interaction requires the presence of a specific 3'UTR (Berkovits and Mayr, 2015; Ma and Mayr, 2018).

Several scenarios can be envisioned how 3'UTRs assist in protein complex formation: They may provide proximity of the interactors or they may change the folding of the nascent peptide chain if the interactor binds in a co-translational manner (Shiber et al., 2018). It is also possible that the protein sequence of BIRC3-LU is post-translationally modified in a 3'UTR-dependent manner which could be the prerequisite for stable binding of some of the 3'UTR-recruited factors. Lastly, the 3'UTR may change the local environment at the site of translation by enabling translation within a specific RNA granule. This was recently shown to be the case for the interaction between CD47 and SET where instead of protein abundance driving the interaction, the local environment found at the site of translation seems to be the crucial determinant of the interaction (Ma and Mayr, 2018).

Interestingly, transfer of proteins from the 3'UTR to the nascent BIRC3 protein may also happen in RNA granules. This view is supported by our single molecule RNA-FISH experiments that showed that *BIRC3* mRNA localizes to RNA foci in the cytoplasm. Furthermore, our data suggest that BIRC3 is translated in these foci as approximately 30% of MS-identified BIRC3 interactors are known components of RNA granules (Elvira et al., 2006). They include ribosomal proteins, translation factors, RNA-binding proteins, DEAD box helicases, and actin-related factors (Figure S3E, Table S2). However, it is currently unclear how these local RNA granules are formed, if their composition differs in a 3'UTR-dependent manner, and if the local RNA granules are required for 3'UTR-dependent protein complex formation.

### **Cooperative binding of RNA-binding proteins throughout the 3'UTR enables specific functions of the long 3'UTR**

RNA-binding proteins mediate diverse functions of 3'UTRs (Mayr, 2017, 2018). A simple explanation how unique functions of long 3'UTRs can be accomplished is through RNA-binding proteins that only bind to the long, but not the short 3'UTR isoform. This was previously shown for the alternative 3'UTRs of *CD47* (Berkovits and Mayr, 2015).

In the case of BIRC3, several RNA-binding proteins interacted with both the short and long 3'UTRs when the short 3'UTR was expressed at high levels. If the same RNA-binding

proteins are able to bind both the short and the long 3' UTR, how can a specific function of the long 3' UTR be achieved? Our data indicate that what matters is the relative amount of HuR bound to the 3' UTR. Only when more HuR than STAU1 was bound, IQGAP1 was recruited by the 3' UTR. The higher HuR amount was achieved through cooperative binding of HuR to several binding sites distributed throughout the entire 3' UTR. This binding mode is especially powerful as a specific function of the long 3' UTR can be achieved, even when the short 3' UTR isoform is expressed at very high levels.

### **Regulation of protein functions by 3' UTR-mediated protein complex formation has the potential to be widespread**

We provide here a strategy for the comprehensive identification of protein interactors using quantitative MS. We validated a number of 3' UTR-dependent BIRC3 interactors that are involved in diverse biological functions. Our data suggests that BIRC3-LU is part of many different stable substoichiometric complexes whose members interact with BIRC3-LU in a 3' UTR-dependent manner. These observations indicate that BIRC3-LU can exert a substantial number of different functions, depending on the nature of the interaction partner.

When comparing 3' UTR isoform ratios between normal and CLL cells, we detected a large number of genes whose mRNA transcripts with long 3' UTRs were upregulated in CLL. As the vast majority of alternative 3' UTR isoform changes did not alter their corresponding mRNA levels, it is likely that instead of protein abundance regulation many 3' UTR ratio changes will enable additional protein functions through 3' UTR-dependent protein complex formation. This suggests that BIRC3 is not the only protein that uses 3' UTR-dependent protein complex formation to gain additional protein functions.

Taken together, in addition to protein functions mediated by 3' UTR-independent interactors whose binding relies solely on features provided by the protein itself, our data reveal that a sizeable fraction of BIRC3 protein complexes require the presence of the long 3' UTR for their formation, but not for the continued maintenance of the complexes. This indicates that in addition to encoding the protein sequence, DNA contains information for protein functions that is transmitted through 3' UTR-dependent protein complex formation (Ma and Mayr, 2018). As 3' UTRs of mRNAs encoding membrane as well as non-membrane proteins are able to form 3' UTR-dependent protein complexes, it is likely that the protein recruitment function of 3' UTRs is widespread. Moreover, as 3' UTR length has expanded during the evolution of higher organisms, 3' UTRs may contribute to their increased biological complexity (Mayr, 2017). This may explain how a limited set of amino acid sequences can accomplish multi-functionality of proteins by using protein complex formation mediated by 3' UTRs.

## **STAR methods text**

### **Samples for 3'-seq and APA analysis**

The normal CD5+ B (NB) cell and the CLL B cell samples were previously published and the 3'-seq data can be accessed in the Gene Expression Omnibus database under the accession numbers GSE111310 and GSE111793 (Singh et al., 2018; Lee et al., 2018). 3/13

CLL samples had a 11q deletion as assessed by FISH. In one sample, the 11q deletion was subclonal, as only 25% of cells showed a heterozygous deletion of 11q. The data were processed as described previously and a significant difference in 3'UTR isoform ratio was determined using a generalized linear model with a false discovery rate (FDR)-adjusted  $P < 0.1$ . The 'short UTR index' (SUI) of an mRNA is calculated as the ratio of reads that map to the proximal polyadenylation site within the 3'UTR divided by all reads that map to the 3'UTR of the mRNA (Lianoglou et al., 2013). A TPM difference ( $> \log_2 1.2$ ) was used to identify differentially expressed mRNAs.

### Cell lines

Raji cells are malignant B cells from lymphomas and were a gift from Dr. Hans-Guido Wendel (MSKCC). HEK293T cells (embryonic kidney) were purchased from ATCC. HeLa cells were provided by Dr. Jonathan Weissman (UCSF). Raji cells were cultured in RPMI with 20% FBS and 1% penicillin/streptomycin. HeLa and HEK293T cells were cultured in DMEM with 10% FBS and 1% penicillin/streptomycin.

### BIRC3 knock-out Raji cells

The pX458 vector, containing Cas9 from *S. pyogenes* with 2A-EGFP and a cloning site for guide RNAs was obtained from Addgene (# 48138) (Ran et al., 2013). The DNA oligonucleotides that served as guide RNAs to produce BIRC3 knock-out Raji cells are listed in Table S4 and were cloned into pX458 vector using the BbsI restriction site.

Raji cells were nucleofected using Nucleofactor V Kit with constructs containing guide RNAs targeting BIRC3. After 24 hours, GFP-positive cells were FACS-sorted into single wells and grown to obtain clones. Knock-out cells were screened using western blots and the positive as well as negative clones were validated using sequencing. The KO3 clone generates a truncated protein with 160 amino acids of BIRC3, followed by a frame-shift mutation that generates 6 additional amino acids followed by a stop codon from one allele and it generates 4 additional amino acids from the other allele (Figure S2A). The KO4 clone generates a truncated protein with 119 amino acids followed by a frame-shift mutation that generates 26 additional amino acids followed by a stop codon from one allele and it generates 8 additional amino acids from the other allele (Figure S2A).

### Constructs

GFP-BIRC3-SU and GFP-BIRC3-LU were cloned into pcDNA3.1 using Gibson Assembly Cloning (New England Biolabs). The primers used for amplification of the pieces are listed in Table S4. The coding region of BIRC3 was amplified from human naïve B cell cDNA and the short or long 3'UTRs were amplified from genomic DNA of human peripheral blood mononuclear cells. GFP-BIRC3-NU does not contain any *BIRC3* 3'UTR, but contains the SV40 polyadenylation signal which is part of the pcDNA3.1 vector.

The GFP constructs that lack the BIRC3 coding region, but contain the 3'UTRs ( CDR-SU, CDR-LU) were generated by replacing the eGFP-BIRC3 fragment in the GFP-BIRC3-SU and GFP-BIRC3-LU constructs by eGFP alone (obtained from pcDNA3.1-puro GFP construct (Ma and Mayr, 2018)).



**Constructs for *in vitro* transcription.**—All *BIRC3* 3'UTR fragments were cloned into pCR-Blunt II-TOPO using SacI and NotI. The antisense constructs were cloned by digesting the sense constructs with NsiI flanking both ends of the 3'UTR fragments. The *LU1* fragment contains 647 nucleotides of the long *BIRC3* 3'UTR and is located between nucleotides 1138 and 1784 of the *BIRC3* 3'UTR. The primers used for PCR amplification are listed in Table S4. The sequence of the ARE was previously described (Ma and Mayr, 2018) and was cloned in the same way as the other 3'UTRs fragments. All the plasmids were linearized using NotI for sense *in vitro* transcription and HindIII for antisense transcription.

The CXCR4 coding region was cloned into pcDNA3.1/myc-His C using EcoRI and NotI sites. The MS2 sequence was described by us before and was inserted into GFP-BIRC3-SU after the stop codon using AgeI and HindIII sites to generate GFP-BIRC3-MS2-SU (Berkovits and Mayr, 2015). The MCP-mCherry (mC) and MCP-mC-HuR constructs were described previously and MCP-mC-STAU1 was generated by replacing HuR using BsrGI and XbaI sites (Berkovits and Mayr, 2015).

For shRNA knock-down experiments pSUPERretropuro (pSUPER) or pSUPER containing eGFP (pSUPER-GFP) was used as described previously (Berkovits and Mayr, 2015). The DNA oligonucleotides used as shRNA precursors are listed in Table S4 and were cloned into pSUPER-GFP or pSUPER. Retroviral particles were generated as described previously (Mayr and Bartel, 2009). For knock-down experiments of IGF2BP1 shRNA constructs were purchased from Sigma (MISSION® shRNA TRCN0000218799, TRCN0000230114). As control an shRNA against luciferase (MISSION® shRNA SHC007) was used.

To generate stable LU KD Raji cell lines, Raji cells were transduced with retrovirus, the culture plates were coated overnight with 5 µg/ml fibronectin. Raji cells were spin-infected containing 8 µg/ml polybrene at 992 g at 30°C for 45 min. The infection procedure was repeated after 48 hours. After cultivating for another two days, the infected cells were selected using 2 µg/ml puromycin. For knockdown of IQGAP1, RALA, STAU1 and HuR, stable cell lines were generated using nucleofection of shRNA constructs using Nucleofactor V Kit (Lonza, Program M-13). After 48 hours, 80% of cells were preserved for FACS analysis and the rest was selected using 2 µg/ml puromycin.

## RNA-FISH

Custom Stellaris EGFP FISH probes were described previously (Berkovits and Mayr, 2015). HeLa cells were plated on 4-well Millicell EZ slide and transfected with GFP fusion constructs. 14 hours after transfection, cells were washed with PBS, fixed with 3.7% formaldehyde for 10 min at room temperature and washed twice for 5 min with PBS. PBS was discarded and 1 ml 70% ethanol was added. The slide was kept at 4°C for 8 hours. The 70% ethanol was aspirated, 1 ml wash buffer was added (2× SSC, 10% formamide in RNase-free water) and incubated at room temperature for 5 min. Hybridization mix was prepared by mixing 10% dextran sulfate, 10% formamide, 2 × SSC, 2 mM ribonucleoside vanadyl complex (NEB), 0.02% BSA, 200 µg/ml yeast tRNA, 200 µg/ml single stranded DNA and FISH probe (1:200). To each well 200 µl hybridization mix was added and hybridized at 37°C overnight. Slides were washed twice for 30 min each with pre-warmed

wash buffer (1 ml, 37°C) in the dark, followed by one quick wash with PBST, and then mounted with mounting solution. Images were captured using confocal ZEISS LSM 880.

### Confocal microscopy

Confocal imaging was performed using a Leica TCS SP8 microscope. HeLa cells were plated on 3.5 cm glass bottom dishes (Cellvis, D35-20-1-N) and allowed to grow overnight. On the next day, the HeLa cells were transfected with GFP-BIRC3-SU or GFP-BIRC3-LU plasmid using Lipofectamine 2000 and were imaged after 24 hours at the Sloan Kettering Institute Molecular Cytology Core Facility.

### Northern blot

Northern blots were performed as previously described (Lianoglou et al., 2013). The template used for generating the BIRC3 probe was PCR amplified from cDNA of human peripheral blood naïve B cells. The primers are listed in Table S4. The levels of the short of long 3'UTR isoforms were quantified using the MultiGauge program (Fuji).

### QRT-PCR

Total RNA was isolated by Tri reagent solution (Invitrogen #AM9738) and digested with DNase I (Invitrogen #AM1906). RNA was reverse transcribed using qScript cDNA SuperMix (Quanta Biosciences #101414-106) and quantitative PCR was performed using FastStart universal SYBR green master mix (Roche) on a 7900HT Fast Real-Time PCR System (Applied Biosystems). The qRT-PCR was performed in triplicates from three independent cDNA preparations.

### Cell viability assay

Ctrl KD, LU KD and BIRC3 KO Raji cells were seeded into 96-well plates and treated with 4 µg/ml Fludarabine. On day 2, 10% (v/v) of Resazurin (R&D Systems, AR002) was added to each well and the plates were incubated for 4 hours at 37°C. The fluorescence in the wells was measured using a microplate reader (SpectraMax M5; Molecular Devices, Sunnyvale, CA, USA) with excitation and emission of 560 nm and 590 nm, respectively. Results were normalized to wells containing media without cells. Each experiment was repeated at least three times with triplicates.

### Migration assay

Raji cells were counted and 100 µl containing  $8 \times 10^5$  cells were added to each transwell (Costar, diameter 6.5 mm, pore size 5 µm). The lower chambers were supplemented with conditioned media containing 50 ng/ml CXCL12 (Life technologies). After 3.5 hours of incubation at 37°C and 5% CO<sub>2</sub>, the migrated cells were collected from the lower chambers and counted manually using Trypan blue. Each biological replicate was performed in triplicates.

### FACS

For surface expression, cells were washed with ice-cold PBS once, incubated with appropriate fluorochrome-conjugated antibodies for 30 min at 4°C and washed twice with

ice-cold PBS containing 0.5% FCS. The following antibodies were used: anti-CD184-APC (CXCR4, 560936, BD Biosciences), anti-CD27-PE (555441, BD Biosciences), anti-CD19-APC (555415, BD Biosciences), anti-CD38-APC (555462, BD Biosciences), anti-CD47-APC (561261, BD Biosciences).

To measure total CXCR4 or CD27 protein level by FACS, Raji cells were fixed with 4% formaldehyde at room temperature for 15 min. After two washes with excess PBS, fixed cells were resuspended with ice-cold PBS and permeabilized with 90% methanol for 10 min on ice. Cells were then washed with cold PBS twice and resuspended with the incubation buffer (PBS + 0.5% BSA). Cells were aliquoted and incubated with anti-CD184-APC or anti-CD27-PE for 20 min at 4°C. After two washes with the incubation buffer, cells were analyzed using a BD FACS Calibur (BD Biosciences) and data were analyzed using the FlowJo software.

### Recycling assay

Raji cells were incubated with 50 ng/ml CXCL12 for 30 min at 37°C and 5% CO<sub>2</sub>. After washing with PBS once, 10% of cells were kept on ice for FACS analysis and the rest of the cells was resuspended in conditioned culture media and incubated at 37°C and 5% CO<sub>2</sub> for an additional 3 hours. All cells were collected and surface CXCR4 expression was analyzed by FACS.

### Co-immunoprecipitation

GFP-BIRC3-SU and GFP-BIRC3-LU were transfected into HEK293T cells using calcium phosphate. After 24 hours, transfected cells were collected and lysed on ice for 30 min with GFP-trap\_A RIPA buffer (Chromotek) containing freshly added proteinase inhibitor cocktail (Thermo Scientific) and phosphatase inhibitors (Sigma). After centrifugation at 21,130 g for 10 min, GFP-trap\_A immunoprecipitation was performed following the manufacturer's instructions. GFP-trap\_A beads were added, incubated with cell lysate for 2 hours at 4°C on a rotator, and washed three times with ice-cold GFP-trap dilution buffer. GFP-trap beads were mixed with 2x Laemmli sample buffer and boiled at 95°C for 5 min. The immunoprecipitates were run on 4-12% Bis-Tris NuPAGE gels using MES running buffer, followed by western blot analysis of the endogenously expressed candidate interactors.

GFP co-IP in the presence of RNase A was performed as described above. RNase A (R4642, Sigma) was added to dilution buffer (1:900) and mixed with cell lysate (final concentration is 1:1500). The mixture was incubated at room temperature for 15 mins, then GFP-trap slurry was added and incubated for another 2.5 hours at 4°C.

*MS2 tethering assay.* The BIRC3-GFP co-IP was performed as described above, but different constructs were used: Instead of GFP-BIRC3-LU, GFP-BIRC3-MS2-SU (containing 24 MS2 binding sites (MS2) after the stop codon) was used. HEK293T cells were transfected with GFP-BIRC3-MS2-SU, MCP-mC-STAU1 and MCP-mC-HuR. This results in tethering of STAU1 and HuR to the short *BIRC3* 3'UTR (Figure 5F, right panel). Tethered STAU1 and HuR recruit endogenously expressed IQGAP1 and RALA to the site of BIRC3 translation, resulting in 3'UTR-dependent protein complex formation between BIRC3, IQGAP1 and RALA, shown by GFP co-IP in Figure 5F, bottom panel. Two control

experiments were performed: GFP-BIRC3-MS2-SU was co-transfected with MCP-mC, followed by GFP co-IP (Figure 5F, left panel). And GFP-BIRC3-SU was co-transfected with MCP-mC-STAU1 and MCP-mC-HuR, followed by GFP- co-IP. In both control experiments IQGAP1 and RALA were unable to interact with BIRC3 protein (Figure 5F, bottom panel). This shows that overexpression of the RNA-binding proteins without tethering to the 3'UTR is not sufficient for 3'UTR-dependent protein complex assembly.

CXCR4-myc co-IP was performed as above with slight modifications. Cells were lysed on ice for 1 hour with CHAPS buffer (50 mM Tris pH 7.4, 150 mM NaCl, 1% Triton X, 1% Na-deoxycholate, 1 mM EDTA, 0.5% CHAPS) with freshly added proteinase inhibitor cocktail and phosphatase inhibitors. After centrifugation of the lysates at 21,130 g for 10 min at 4°C, the supernatant was collected and pre-cleared using 20 µl Protein A/G PLUS-Agarose beads (sc-2003, SCBT) for 1.5 hours at 4°C with rotation. The pre-cleared lysates were incubated with 1 µg of anti-MYC antibody (Sigma, M4439) or IgG (IgG, sc-2025, SCBT) for 2 hours at 4°C with rotation, then 20 µl of agarose beads were added and the reaction was rotated for an additional 45 min at 4°C. After washing the beads three times with wash buffer (50 mM Tris pH 7.4, 150 mM NaCl, 1 mM EDTA, freshly added proteinase inhibitor cocktail), beads were mixed with 2x Laemmli sample buffer (Sigma), followed by western blot analysis.

### Quantitative mass spectrometry

GFP-trap co-IP was performed with slight modifications. HEK293T cells were cultivated in DMEM medium supplemented with 10% FBS and 1% penicillin and containing either “light” (L-Arginine-HCL) or “heavy” (L- Arginine-HCL (13C6, 99%; 15N4, 99%; Cambridge Isotope Laboratories, CNLM-539-H-0.05) stable isotope labeled amino acids. Cells were cultivated for at least six passages before the incorporation efficiency was verified by mass spectrometry analysis. The ‘light’ HEK293T cells were transfected with GFP-BIRC3-SU and the ‘heavy’ cells were transfected with GFP-BIRC3-LU using calcium phosphate. After 24 hours, transfected cells were collected and lysed on ice for 30 min and lysates from the light and heavy samples were pooled, followed by GFP-trap co-IP. The beads were mixed with 2x Laemmli sample buffer followed by SDS-gel electrophoresis in MES running buffer using 4-12% Bis-Tris NuPAGE gels. The protein gels were stained with SimplyBlue (Life technologies) following manufacturer’s instructions and submitted to the MSKCC Proteomics Core facility for SILAC mass spectrometry analysis.

Mass spectrometry was performed as was described previously (Shevchenko et al., 2006). Gel slices were then washed with 1:1 (Acetonitrile: 100 mM ammonium bicarbonate) for 30 min, dehydrated with 100% acetonitrile for 10 min, excess acetonitrile was removed and slices were dried in speed-vac for 10 min without heat. Gel slices were reduced with 5 mM DTT for 30 min at 56°C in a thermomixer (Eppendorf) and chilled down to room temperature, and alkylated with 11 mM IAA for 30 min in the dark. Gel slices were washed with 100 mM ammonium bicarbonate and 100% acetonitrile for 10 min each. Excess acetonitrile was removed and dried in speed-vac for 10 min without heat and gel slices were rehydrated in a solution of 25 ng/µl trypsin in 50 mM ammonium bicarbonate on ice for 30 min. Digestions were performed overnight at 37°C in a thermomixer. Digested peptides were

collected and further extracted from gel slices in extraction buffer (1:2 (v/v) 5% formic acid/ acetonitrile) at high speed shaking in a thermomixer. Supernatant from both extractions was combined and dried in a vacuum centrifuge. Peptides were desalted with C18 resin-packed stage-tips, lyophilized and stored at  $-80^{\circ}\text{C}$  until further use.

**LC-MS/MS analysis:** Desalted peptides were dissolved in 3% acetonitrile/0.1% formic acid and were injected onto a C18 capillary column on a nano ACQUITY UPLC system (Water) which was coupled to the Q Exactive plus mass spectrometer (Thermo Scientific). Peptides were eluted with a non-linear 200 min gradient of 2-35% buffer B (0.1% (v/v) formic acid, 100% acetonitrile) at a flow rate of 300 nl/min. After each gradient, the column was washed with 90% buffer B for 5 min and re-equilibrated with 98% buffer A (0.1% formic acid, 100% HPLC-grade water). MS data were acquired with an automatic switch between a full scan and 10 data-dependent MS/MS scans (TopN method). Target value for the full scan MS spectra was  $3 \times 10^6$  ions in the 380-1800  $m/z$  range with a maximum injection time of 30 ms and resolution of 70,000 at 200  $m/z$  with data collected in profile mode. Precursors were selected using a 1.5  $m/z$  isolation width. Precursors were fragmented by higher-energy C-trap dissociation (HCD) with a normalized collision energy of 27 eV. MS/MS scans were acquired at a resolution of 17,500 at 200  $m/z$  with an ion target value of  $5 \times 10^4$ , maximum injection time of 60 ms, dynamic exclusion for 15 s and data collected in centroid mode.

To generate protein IDs and SILAC ratios all .raw data were analyzed by using MaxQuant (Max Planck Institute of Biochemistry; version 1.5.1.0) at default settings with first search tolerance and main search tolerance of 20 ppm and 6 ppm, respectively. Data were further analyzed by Scaffold 4 version 4.5. Only proteins with a least two different peptides were considered for analysis and the  $\log_2$  ratio of the heavy versus the light fraction (LU/SU) was calculated. This showed equal abundance of BIRC3 in the heavy versus the light fraction as the  $\log_2$  enrichment ratio was 0.033 (which corresponds to a ratio of 1.02). A cut-off of  $\log_2$  0.585 (1.5-fold) was used to identify the BIRC3-LU-enriched protein interaction partners. The 3'UTR-independent interactors had a  $\log_2$  LU/SU ratio  $<0.585$ .

### Gene ontology analysis

Gene ontology analysis was performed using DAVID 6.8 (Huang da et al., 2009). The enrichment scores and corresponding  $p$  values of the functional categories that were exclusively enriched in either the 3'UTR-independent or 3'UTR-dependent (BIRC3-LU-enriched) interactors are reported.

### Western blot analysis

Cells were lysed on ice for 30 min with RIPA buffer (50 mM Tris pH 7.4, 150 mM NaCl, 1% NP-40, 1% Na-deoxycholate, 1 mM EDTA, 0.05% SDS). Lysates were cleared using centrifugation at maximum speed, mixed with 2x Laemmli sample buffer (Sigma), boiled at  $95^{\circ}\text{C}$  for 5 min, and chilled on ice for 1 min before loading on gels. For CXCR4 analyses, cells were lysed on ice for 1 hour with CHAPS buffer containing proteinase inhibitor cocktail and phosphatase inhibitors. Lysates were cleared using centrifugation at max speed, mixed with 2x Laemmli sample buffer (Sigma) and incubated at  $37^{\circ}\text{C}$  for 1 hour. Lysates

were run using 4-12% Bis-Tris NuPAGE gels (Life technologies) with MES running buffer (Natural Diagnostics or Life technologies). The separated proteins were transferred to nitrocellulose membranes (1620252, Bio-Rad), blocked with Odyssey Blocking Buffer (Li-Cor, 927-40000) for 1 hour at room temperature, followed by incubation with primary antibodies at 4°C overnight. After two washes using PBS and 0.1% Tween 20 (PBST), the blots were incubated with IRDye-conjugated secondary antibodies for 50 min at room temperature. After one wash with PBST and two washes with PBS, proteins were detected with Odyssey CLx imaging system (Li-Cor).

The following primary antibodies were used: anti-ACTIN (A4700, Sigma, A2066, Sigma), anti-GFP (ab13970, Abcam), anti-DIABLO (2954, Cell Signaling), anti-XIAP (2042, Cell Signaling), anti-SMARCA4 (BRG1, 3508, Cell Signaling), anti-SMARCA5 (SNF2H, 38410, Cell Signaling), anti-HSPA9 (SAB4100033, Sigma), anti-TIMM44 (ab194829, Abcam), anti-IQGAP1 (SAB4200079, Sigma), anti-RALA (ab126627, Abcam), anti-BAZ1B (sc-514287, SCBT), anti-ATP5B (ab14730, Abcam), anti-MYC (M4439, Sigma), anti-BIRC3 (3130P, Cell Signaling), anti-mCherry (ab125096, Abcam), anti-CXCR4 (4G10, sc-53534, SCBT), anti-ELAVL1 (HuR, 07-1735, Millipore), anti-STAU1 (14225-1-AP, Proteintech), anti-IGF2BP1 (ARP40658\_P050, Aviva Systems Biology), anti-hnRNPA1 (sc-374526, SCBT), anti-hnRNPQ (R5653, Sigma), anti-CTR9 (SAB1100738, Sigma), anti-YBX1 (A303-231A-M, Bethyl Laboratories), anti-SF3B1 (D221-3, Medical & Biological Laboratories Co., LTD), anti-NUDT21 (sc-81109, SCBT), anti-FUS (SAB4200478, Sigma), anti-KHSRP (SAB4200566, Sigma), anti-hnRNPC (sc-32308, SCBT), anti-DDX17 (ab24601, Abcam), and anti-snRNP70 (sc-9571, SCBT).

The secondary antibodies used included anti-mouse IRDye 700 (610-730-002, Rockland Immunochemicals), anti-rabbit IRDye 680 (926-68073, Li-Cor Biosciences), anti-rabbit IRDye 800 (926-32213, Li-Cor Biosciences), and anti-mouse IRDye 800 (926-32212, Li-Cor Biosciences).

### RNA affinity pull-down assay

This assay was performed as before with modifications as outlined below (Panda et al., 2016). After linearization of the plasmids the DNA templates were purified by Phenol:Chloroform extraction, followed by ethanol precipitation containing sodium acetate. *In vitro* transcription was performed according to the manufacturer's instructions (MEGAscript T7, Invitrogen). In the mixture, 0.5 µg of linearized DNA template was used and Biotin-UTP (AM8450, Invitrogen) was added to biotin-label the RNAs. The ratio of the ribonucleotide solutions was ATP:CTP:GTP:UTP:Biotin-UTP = 1: 0.9: 0.9: 0.945: 0.055). After labeling, the RNAs were recovered using Phenol:Chloroform extraction and isopropanol precipitation. The RNAs were stored at -80°C until further use.

The amount of RNAs to incubate with cell lysate was determined by first measuring the RNA concentrations using Nanodrop, followed by agarose gel analysis to confirm the concentrations. The same molar amount of RNA molecules were used for RNA affinity pull-down reactions, if not stated otherwise.



Biotinylated RNAs were thawed on ice and boiled at 95°C for 2 minutes, slowly cooled down to room temperature and then were kept on ice. HEK293T cells or Raji cells were lysed in lysis buffer (20 mM Tris-HCL pH 7.5, 250 mM NaCl, 50 mM KCl, 2.5 mM MgCl<sub>2</sub>, 0.25% NP-40, 0.5% Triton X-100, 1 mM EDTA pH 8 with 1x protease inhibitor). One 10 cm<sup>2</sup> dish of cells (about 30 million of Raji cells) was used for one pull-down reaction. Each dish was washed with cold PBS twice and lysed with 500 µl lysis buffer on ice for 20 minutes. Cell lysate was collected after spinning at 21,000 × g for 10 minutes at 4°C. Pull-down mixture was prepared as follows: 450 µl of cell lysate (keep 30 µl as input for western blot), 1 µg of LU RNA (same molar amounts of the other 3' UTR RNAs), and 0.2 U/ml of RNaseOUT. The reactions were incubated at 4°C for 1.5 hours with rotation. Meanwhile, Dynabeads® MyOne™ Streptavidin C1 (65002, Invitrogen) were washed with wash buffer (10 mM Tris-HCL pH 7.5, 250 mM NaCl, 0.5% Triton X-100, 1 mM EDTA pH 8 with 1x protease inhibitor). After three washes, 50 µl of beads were added to each pull-down reaction and the mixtures were incubated for another 40 minutes. The pull-down beads were washed 5 times with wash buffer and resuspended with 2x sample buffer (Sigma). All samples were boiled at 95°C for 2 min, incubated on ice for 1 min, and half of the sample was loaded onto NuPage gel for western blot analysis.

### Statistical tests

To test for differences in cell viability a t-test for independent samples was used (equal variance was not assumed). For pairwise comparisons a Mann Whitney test was performed. If more than two samples were tested, first a Kruskal Wallis test was applied.

### Supplementary Material

Refer to Web version on PubMed Central for supplementary material.

### Acknowledgements

We thank the MSKCC Proteomics Facility for performing the mass spectrometry experiments and the Molecular Cytology Facility for help with the imaging. We thank all members of the Mayr lab for helpful discussions and Dirk Remus and Sibylle Mitschka for critical reading of the manuscript. This work was funded by the NIH Director's Pioneer Award (DP1-GM123454), the Damon Runyon Innovator Award, the Pershing Square Sohn Cancer Research Alliance, and the NCI Cancer Center Support Grant (P30 CA008748).

### References

- Bamidele AO, Kremer KN, Hirsova P, Clift IC, Gores GJ, Billadeau DD, and Hedin KE (2015). IQGAP1 promotes CXCR4 chemokine receptor function and trafficking via EEA-1+ endosomes. *The Journal of cell biology* 210, 257–272. [PubMed: 26195666]
- Berkovits BD, and Mayr C (2015). Alternative 3' UTRs act as scaffolds to regulate membrane protein localization. *Nature* 522, 363–367. [PubMed: 25896326]
- Beug ST, Cheung HH, LaCasse EC, and Korneluk RG (2012). Modulation of immune signalling by inhibitors of apoptosis. *Trends in immunology* 33, 535–545. [PubMed: 22836014]
- Brumbaugh J, Di Stefano B, Wang X, Borkent M, Forouzmand E, Clowers KJ, Ji F, Schwarz BA, Kalocsay M, Elledge SJ, et al. (2018). Nudt21 Controls Cell Fate by Connecting Alternative Polyadenylation to Chromatin Signaling. *Cell* 172, 629–631. [PubMed: 29373832]
- Burger M, Hartmann T, Krome M, Rawluk J, Tamamura H, Fujii N, Kipps TJ, and Burger JA (2005). Small peptide inhibitors of the CXCR4 chemokine receptor (CD184) antagonize the activation,

- migration, and antiapoptotic responses of CXCL12 in chronic lymphocytic leukemia B cells. *Blood* 106, 1824–1830. [PubMed: 15905192]
- Elvira G, Wasiaik S, Blandford V, Tong XK, Serrano A, Fan X, del Rayo Sanchez-Carbente M, Servant F, Bell AW, Boismenu D, et al. (2006). Characterization of an RNA granule from developing brain. *Molecular & cellular proteomics : MCP* 5, 635–651. [PubMed: 16352523]
- Geisbrecht ER, and Montell DJ (2004). A role for Drosophila IAP1-mediated caspase inhibition in Rac-dependent cell migration. *Cell* 118, 111–125. [PubMed: 15242648]
- Gruber AR, Martin G, Muller P, Schmidt A, Gruber AJ, Gumienny R, Mittal N, Jayachandran R, Pieters J, Keller W, et al. (2014). Global 3' UTR shortening has a limited effect on protein abundance in proliferating T cells. *Nature communications* 5, 5465.
- Grundler R, Brault L, Gasser C, Bullock AN, Dechow T, Woetzel S, Pogacic V, Villa A, Ehret S, Berridge G, et al. (2009). Dissection of PIM serine/threonine kinases in FLT3-ITD-induced leukemogenesis reveals PIM1 as regulator of CXCL12-CXCR4-mediated homing and migration. *The Journal of experimental medicine* 206, 1957–1970. [PubMed: 19687226]
- Huang da W, Sherman BT, and Lempicki RA (2009). Systematic and integrative analysis of large gene lists using DAVID bioinformatics resources. *Nature protocols* 4, 44–57. [PubMed: 19131956]
- Huttlin EL, Bruckner RJ, Paulo JA, Cannon JR, Ting L, Baltier K, Colby G, Gebreab F, Gygi MP, Parzen H, et al. (2017). Architecture of the human interactome defines protein communities and disease networks. *Nature* 545, 505–509. [PubMed: 28514442]
- Jia X, Yuan S, Wang Y, Fu Y, Ge Y, Ge Y, Lan X, Feng Y, Qiu F, Li P, et al. (2017). The role of alternative polyadenylation in the antiviral innate immune response. *Nature communications* 8, 14605.
- Lee SH, Singh I, Tisdale S, Abdel-Wahab O, Leslie CS, and Mayr C (2018). Widespread intronic polyadenylation inactivates tumour suppressor genes in leukaemia. *Nature* 561, 127–131. [PubMed: 30150773]
- Lianoglou S, Garg V, Yang JL, Leslie CS, and Mayr C (2013). Ubiquitously transcribed genes use alternative polyadenylation to achieve tissue-specific expression. *Genes Dev* 27, 2380–2396. [PubMed: 24145798]
- Ma W, and Mayr C (2018). A Membraneless Organelle Associated with the Endoplasmic Reticulum Enables 3'UTR-Mediated Protein-Protein Interactions. *Cell* 175, 1492–1506 e1419. [PubMed: 30449617]
- Marchese A (2016). Monitoring Chemokine Receptor Trafficking by Confocal Immunofluorescence Microscopy. *Methods in enzymology* 570, 281–292. [PubMed: 26921951]
- Mayr C (2017). Regulation by 3'-Untranslated Regions. *Annual review of genetics* 51, 171–194.
- Mayr C (2018). What Are 3' UTRs Doing? *Cold Spring Harb Perspect Biol*.
- Mayr C, and Bartel DP (2009). Widespread shortening of 3'UTRs by alternative cleavage and polyadenylation activates oncogenes in cancer cells. *Cell* 138, 673–684. [PubMed: 19703394]
- Neyraud V, Aushev VN, Hatzoglou A, Meunier B, Cascone I, and Camonis J (2012). RalA and RalB proteins are ubiquitinated GTPases, and ubiquitinated RalA increases lipid raft exposure at the plasma membrane. *J Biol Chem* 287, 29397–29405. [PubMed: 22700969]
- Panda AC, Martindale JL, and Gorospe M (2016). Affinity Pulldown of Biotinylated RNA for Detection of Protein-RNA Complexes. *Bio-protocol* 6.
- Ran FA, Hsu PD, Wright J, Agarwala V, Scott DA, and Zhang F (2013). Genome engineering using the CRISPR-Cas9 system. *Nature protocols* 8, 2281–2308. [PubMed: 24157548]
- Rose-Zerilli MJ, Forster J, Parker H, Parker A, Rodriguez AE, Chaplin T, Gardiner A, Steele AJ, Collins A, Young BD, et al. (2014). ATM mutation rather than BIRC3 deletion and/or mutation predicts reduced survival in 11q-deleted chronic lymphocytic leukemia: data from the UK LRF CLL4 trial. *Haematologica* 99, 736–742. [PubMed: 24584352]
- Rossi D, Fangazio M, Rasi S, Vaisitti T, Monti S, Cresta S, Chiaretti S, Del Giudice I, Fabbri G, Brusca A, et al. (2012). Disruption of BIRC3 associates with fludarabine chemorefractoriness in TP53 wild-type chronic lymphocytic leukemia. *Blood* 119, 2854–2862. [PubMed: 22308293]
- Sandberg R, Neilson JR, Sarma A, Sharp PA, and Burge CB (2008). Proliferating cells express mRNAs with shortened 3' untranslated regions and fewer microRNA target sites. *Science* 320, 1643–1647. [PubMed: 18566288]

- Shevchenko A, Tomas H, Havlis J, Olsen JV, and Mann M (2006). In-gel digestion for mass spectrometric characterization of proteins and proteomes. *Nature protocols* 1, 2856–2860. [PubMed: 17406544]
- Shiber A, Doring K, Friedrich U, Klann K, Merker D, Zedan M, Tippmann F, Kramer G, and Bukau B (2018). Cotranslational assembly of protein complexes in eukaryotes revealed by ribosome profiling. *Nature*.
- Singh I, Lee SH, Sperling AS, Samur MK, Tai YT, Fulciniti M, Munshi NC, Mayr C, and Leslie CS (2018). Widespread intronic polyadenylation diversifies immune cell transcriptomes. *Nature communications* 9, 1716.
- Spies N, Burge CB, and Bartel DP (2013). 3' UTR-isoform choice has limited influence on the stability and translational efficiency of most mRNAs in mouse fibroblasts. *Genome Res* 23, 2078–2090. [PubMed: 24072873]
- Sugimoto Y, Vigilante A, Darbo E, Zirra A, Militti C, D'Ambrogio A, Luscombe NM, and Ule J (2015). hiCLIP reveals the in vivo atlas of mRNA secondary structures recognized by Stauf1. *Nature* 519, 491–494. [PubMed: 25799984]
- Sutton LA, and Rosenquist R (2015). The complex interplay between cell-intrinsic and cell-extrinsic factors driving the evolution of chronic lymphocytic leukemia. *Seminars in cancer biology* 34, 22–35. [PubMed: 25963298]
- Villace P, Marion RM, and Ortin J (2004). The composition of Stauf1-containing RNA granules from human cells indicates their role in the regulated transport and translation of messenger RNAs. *Nucleic Acids Res* 32, 2411–2420. [PubMed: 15121898]
- Zhang KX, Tan L, Pellegrini M, Zipursky SL, and McEwen JM (2016). Rapid Changes in the Transcriptome during the Conversion of Growth Cones to Synaptic Terminals. *Cell reports* 14, 1258–1271.

**Highlights:**

- The long *BIRC3* 3'UTR isoform is upregulated in leukemia
- Quantitative mass spectrometry identifies 3'UTR-dependent BIRC3 protein interactors
- The long 3'UTR is required for the formation of several BIRC3 protein complexes
- BIRC3 is cancer-promoting through control of CXCR4 trafficking and B cell migration

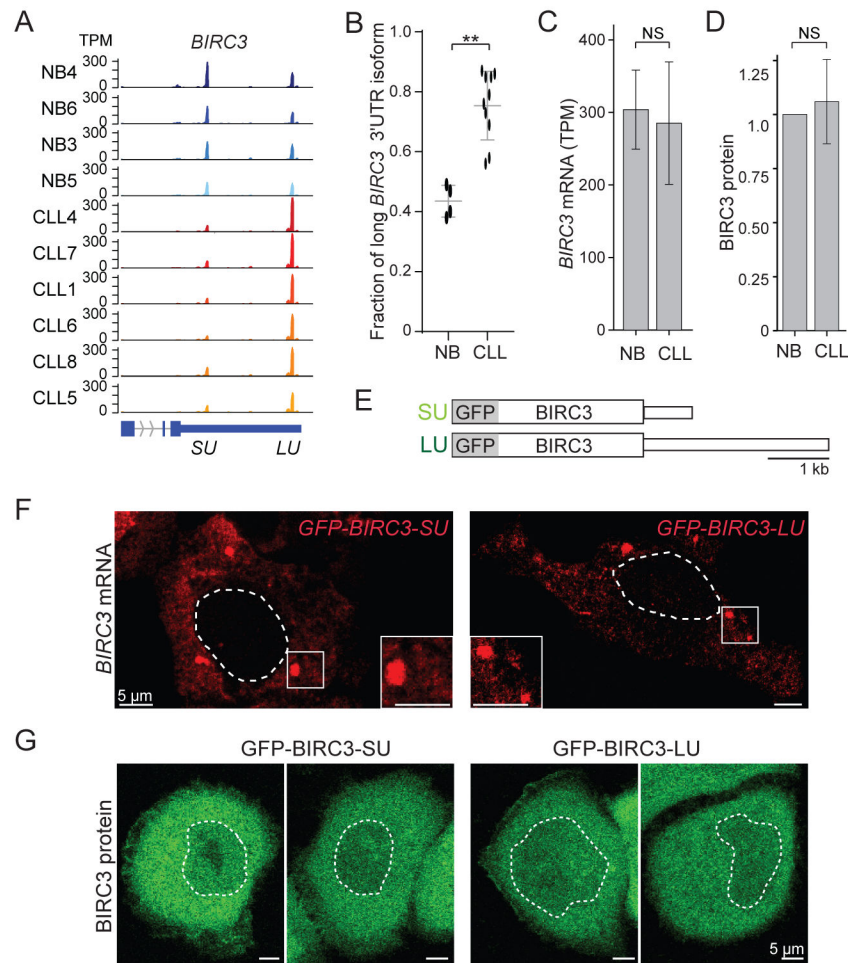


**Figure 1. The alternative *BIRC3* 3' UTRs do not regulate *BIRC3* protein abundance or localization.**

(A) The short and long *BIRC3* 3' UTRs are shown as 3'-seq data in transcripts per million (TPM) for normal CD5+ B cells (NB) and CLL B cells. The terminal exons are shown in blue. *SU*, short 3' UTR, *LU*, long 3' UTR.

(B) Fraction of long *BIRC3* 3' UTR isoform in normal ( $N = 4$ ) and CLL B ( $N = 10$ ) cells as mean  $\pm$  SD, Mann Whitney test, \*\*,  $p = 0.003$ .

(C) Overall *BIRC3* mRNA abundance of samples from (B). Mann Whitney test,  $p = \text{NS}$  (not significant).

(D) *BIRC3* protein level quantification from Figure S1D. Mann Whitney test,  $p = \text{NS}$ .

(E) Constructs: GFP fusion with *BIRC3* coding region, followed by either the short (*SU*) or long (*LU*) *BIRC3* 3' UTR.

(F) Single molecule RNA-FISH against GFP after transfection of constructs from (E) in HeLa cells. The dotted line demarcates the nucleus. Representative cells are presented.

(G) Live cell fluorescence microscopy shows GFP-*BIRC3* protein as in (F).

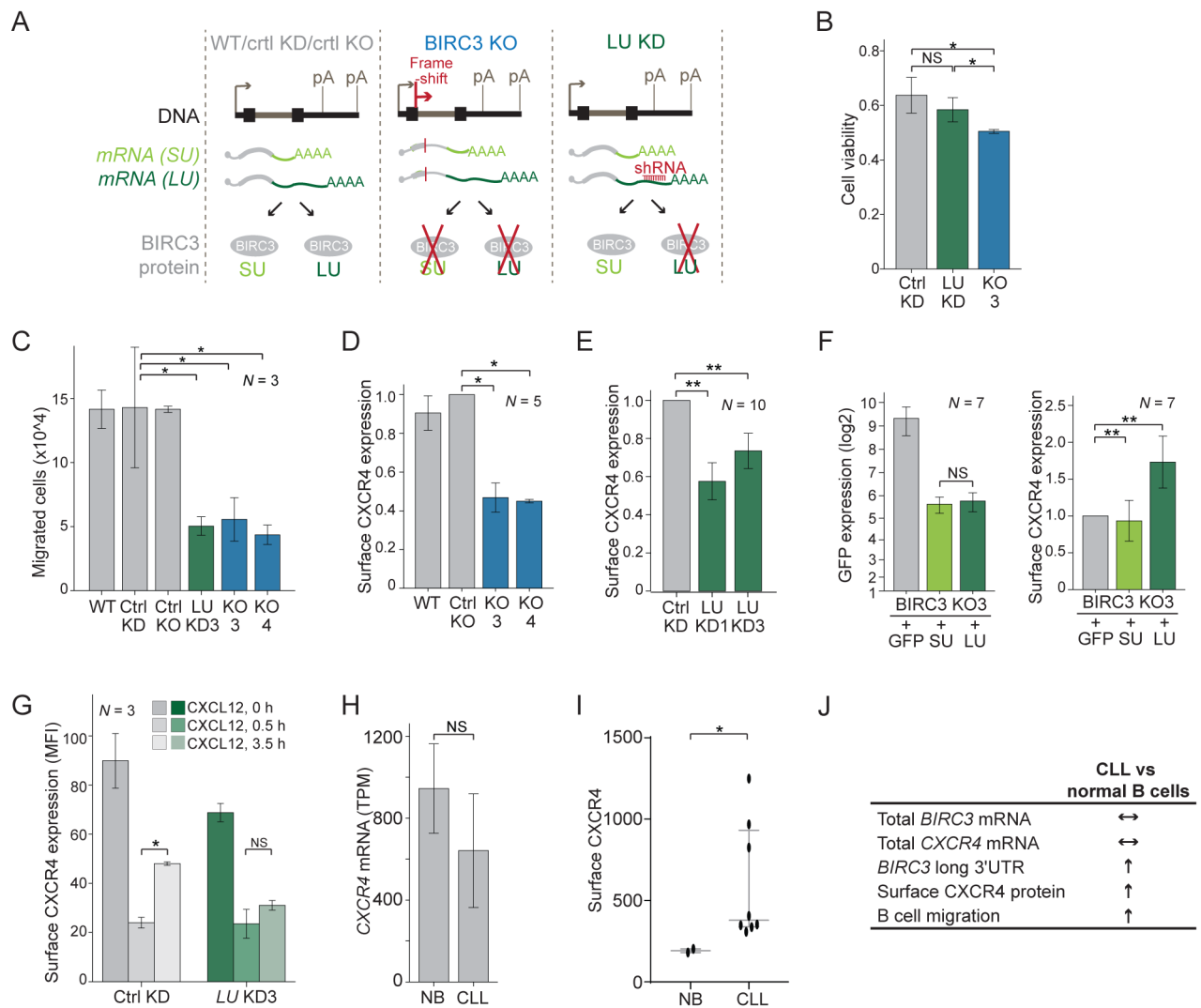


**Figure 2. 3'UTR-independent and 3'UTR-dependent functions of BIRC3.**

**(A)** Experimental systems for phenotypic analysis. Raji cells ( $N = 2$ ) with BIRC3 protein knock-out (KO). Controls: parental Raji cells (WT) and Raji clone after CRISPR procedure that retains BIRC3 protein (ctrl KO). Raji cells with stable expression of shRNAs against the long *BIRC3* 3'UTR isoform (LU KD,  $N = 2$ ) are compared to cells expressing a control shRNA (ctrl KD). Arrow indicates transcriptional start and pA indicates polyadenylation signal.

**(B)** Viability at day 2 after Fludarabine treatment for biological replicates of ctrl Raji ( $N = 4$ ), LU KD ( $N = 4$ ), and BIRC3 KO cells ( $N = 2$ ). T-test for independent samples, \*,  $p < 0.039$ .

**(C)** B cell migration after 3.5 hours in media with 50 ng/ml CXCL12 as mean  $\pm$  SD from biological replicates. Mann Whitney test, \*,  $p = 0.02$ .

**(D)** FACS analysis of endogenous surface CXCR4 expression in ctrl and KO cells as mean fluorescence intensity (MFI)  $\pm$  SD of biological replicates. Mann Whitney test, \*,  $p = 0.03$ . Representative example in Figure S2J.



- (E)** As in (D), but for ctrl and LU KD cells. Mann Whitney test, \*\*,  $p = E-5$ . Representative example in Figure S2K.
- (F)** FACS analysis of endogenous surface CXCR4 levels in KO3 cells after expression of constructs from Figure 1E. GFP expression in left panel and mean MFI of surface CXCR4  $\pm$  SD from biological replicates in right panel. Mann Whitney test, \*\*,  $p = 0.003$ . Representative example in Figure S2L.
- (G)** FACS analysis of endogenous surface CXCR4 levels from Figure S2M. Shown is mean MFI  $\pm$  SD from biological replicates. Mann Whitney test, \*,  $p = 0.03$ .
- (H)** *CXCR4* mRNA level of NB ( $N = 4$ ) and CLL B ( $N = 10$ ) as mean 3'-seq TPM  $\pm$  SD. Mann Whitney test,  $p = NS$ .
- (I)** FACS analysis of endogenous surface CXCR4 shown as MFI  $\pm$  SD for normal ( $N = 2$ ) and CLL B ( $N = 8$ ) cells. Mann Whitney test, \*,  $p = 0.037$ .
- (J)** 3'UTR-dependent trafficking regulation by BIRC3 is important for CLL biology. Similar mRNA level of *BIRC3* and *CXCR4*, but increased expression of the long *BIRC3* 3'UTR in CLL which correlates with increased surface CXCR4 protein, allowing CLL cell migration towards the CXCL12 cytokine expressed in bone marrow niches.

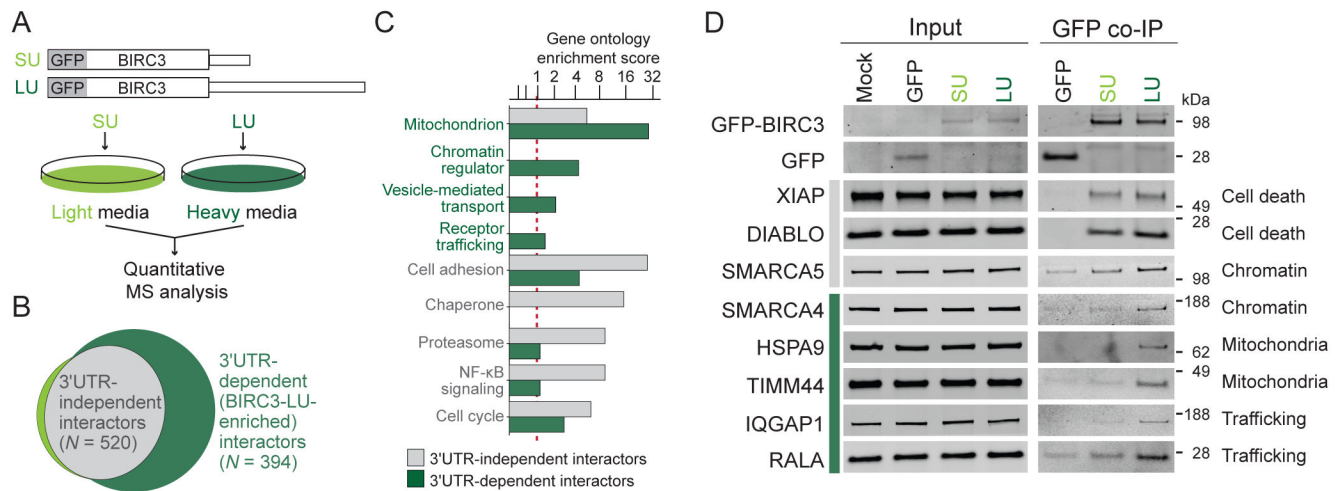


**Figure 3. Identification and validation of 3'UTR-independent and 3'UTR-dependent BIRC3 protein interactors.**

(A) Experimental set-up: HEK293T cells are grown in heavy and light SILAC media, transfected with GFP-BIRC3-LU and GFP-BIRC3-SU, pooled, immunoprecipitated using GFP-trap, and co-IPed proteins are analyzed by MS.

(B) Interactors are classified as 3'UTR-independent (shared by BIRC3-SU and BIRC3-LU;  $\log_2$  LU/SU ratio  $<0.585$ ; grey) and long 3'UTR-dependent (BIRC3-LU-enriched;  $\log_2$  LU/SU ratio  $>0.585$ ). See also Table S2.

(C) Gene ontology enrichment score from interactors identified in (B). Red dotted line is cut-off for enrichment.

(D) Western blot validation of endogenous BIRC3 interactors. 3'UTR-independent (grey bar) and 3'UTR-dependent (green bar) BIRC3 protein interactors identified by GFP co-IP in HEK293T cells after transfection of constructs from Figure 1E. 1% of input was loaded.

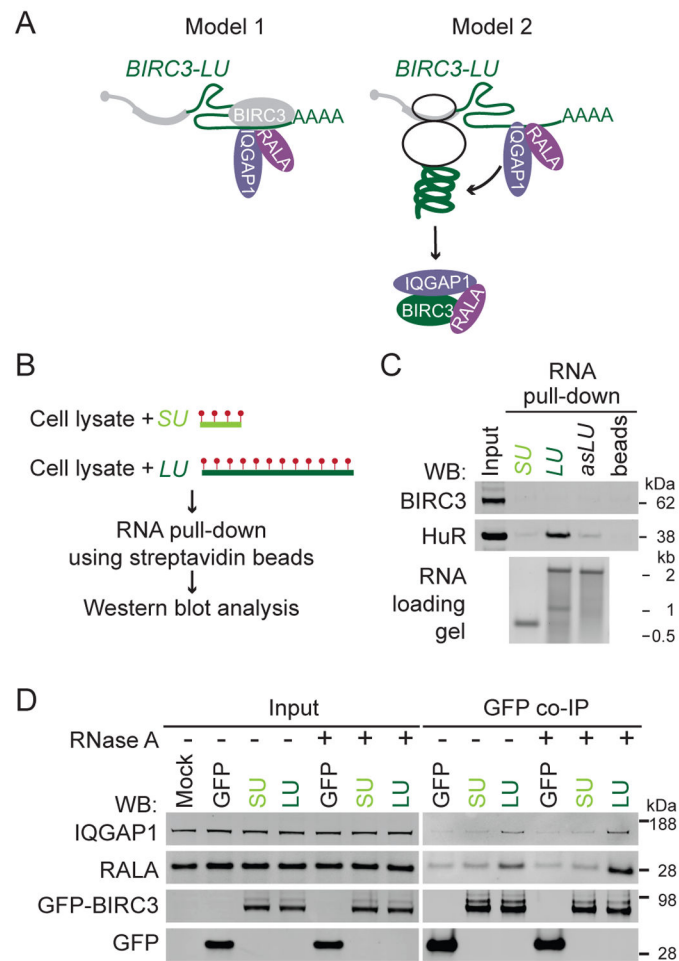


**Figure 4. The long *BIRC3* 3'UTR of is required for establishment but not maintenance of 3'UTR-dependent *BIRC3* protein complexes.**

(A) Models for 3'UTR-dependent protein complex formation. See text for details.

(B) Experimental set-up for RNA affinity pull-down to identify RNA-binding proteins that bind to the alternative 3'UTRs of *BIRC3*. Biotinylated uridines (red dots) are incorporated during *in vitro* transcription of the 3'UTRs. After incubation with Raji cell lysate, the RNAs together with bound RNA-binding proteins are pulled-down using streptavidin beads. Visualization of endogenously expressed RNA-binding proteins by western blot.

(C) RNA affinity pull-down described in (B). Western blot of endogenous *BIRC3* and HuR after pull-down of the short *BIRC3* 3'UTR (SU), the long *BIRC3* 3'UTR (LU), the antisense (as) sequence of LU, and of beads only. 2% of input was loaded. The same number of RNA molecules was incubated with lysate. HuR serves as positive control (see Figure 5A).

(D) As in Figure 3D. GFP co-IP was performed in the presence or absence of RNase A.

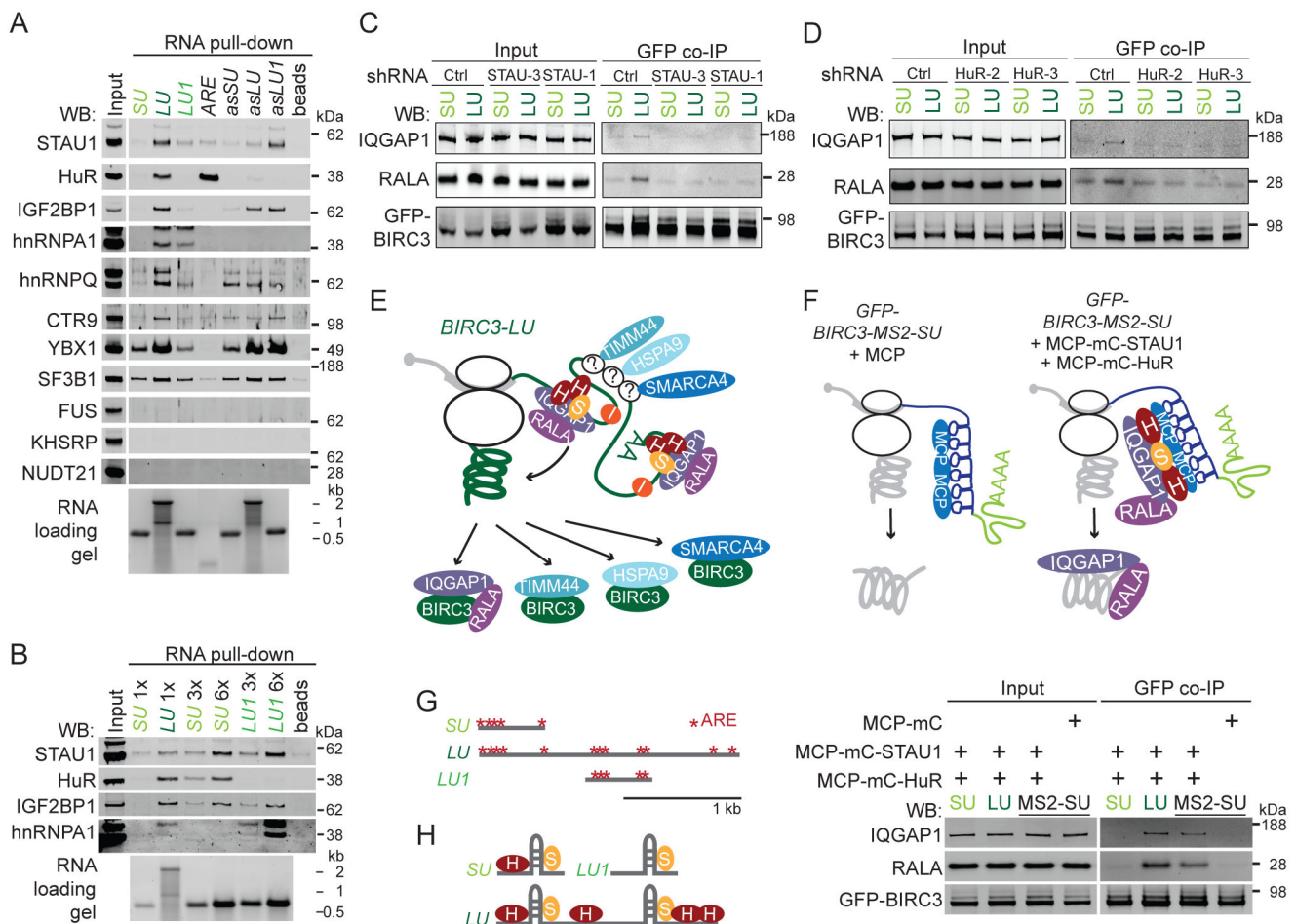


**Figure 5. The RNA-binding proteins STAU1 and HuR recruit the 3'UTR-dependent protein interactors IQGAP1 and RALA.**

(A) As in Figure 4C, but performed in HEK293T cells. *LU1*, fragment of the long *BIRC3* 3'UTR (see (G)). *ARE* is a repeated AU-rich element that serves as positive control for HuR. RNA-binding proteins involved in mRNA processing are SF3B1, KHSRP, NUDT21, hnRNPC, DDX17, and snRNP70 (shown in Figure S5C).

(B) As in (A), but indicated amounts of biotinylated RNAs were incubated with lysate.

(C) As in Figure 4D, but after stable expression of ctrl shRNAs or shRNAs against STAU1 (STAU-1, STAU-3).

(D) As in (C), but after stable expression of shRNAs against HuR (HuR-2, HuR-3).

(E) Model how different RNA-binding proteins recruit different 3'UTR-dependent interactors. IQGAP1 and RALA are recruited by STAU1 (S) and HuR (H) and not by IGF2BP1 (I). The RNA-binding proteins that recruit HSPA9, TIMM44, and SMARCA4 are unknown (indicated by '?').

(F) *In vivo* reconstitution of IQGAP1/RALA recruitment to BIRC3 protein by STAU1 and HuR tethered to the short 3'UTR. See text and methods for details. GFP co-IP of IQGAP1 and RALA after transfection of GFP-BIRC3-SU (SU), GFP-BIRC3-LU (LU), or GFP-BIRC3-MS2-SU (MS2-SU) into HEK293T cells. MCP-mC-STAU1 and MCP-mC-HuR

were cotransfected in the indicated lanes (see Figure S5H). They recruit endogenously expressed IQGAP1 and RALA. 1 % of input was loaded.

**(G)** AU-rich elements (AREs, red stars) located in the alternative *BIRC3* 3' UTRs. *LU1* is a 647 nucleotide fragment derived from the long *BIRC3* 3' UTR that contains five AREs.

**(H)** The ratio of the RNA-binding proteins STAU1 and HuR bound to the alternative *BIRC3* 3' UTRs is important for the BIRC3-LU-specific recruitment of IQGAP1 and RALA. STAU1 binds to double-stranded RNA. The model is based on the data shown in (B).

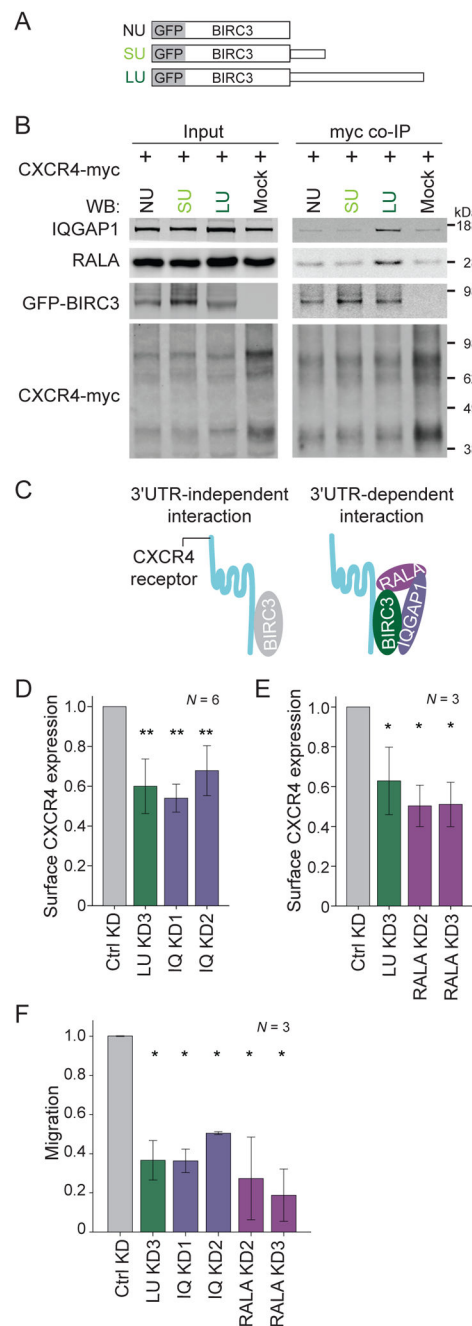


**Figure 6. IQGAP1 and RALA are recruited to CXCR4 in a BIRC3-LU-dependent manner and regulate surface CXCR4 expression and B cell migration.**

(A) Constructs as in Figure 1E and GFP fusion with BIRC3 coding region, followed by no 3'UTR (NU; but the construct includes a polyadenylation signal).

(B) Myc co-IP of endogenous IQGAP1 and RALA after transfection of CXCR4-myc and the constructs from (A) into HEK293T cells. 4.5 % of input was loaded. Quantification in Figure S6A.

(C) Model of 3'UTR-independent interaction between BIRC3 and CXCR4, which can be accomplished by BIRC3-NU, BIRC3-SU or BIRC3-LU. The 3'UTR-dependent interaction



happens between BIRC3-LU, IQGAP1, RALA, and CXCR4 and can only be accomplished by BIRC3-LU.

**(D)** FACS analysis of endogenous surface CXCR4 levels in Raji cells stably expressing a ctrl shRNA or shRNAs against IQGAP1 (IQ KD). LU KD is shown for comparison reasons. MFI  $\pm$  SD from biological replicates. Mann Whitney test, ctrl KD vs each sample, \*\*,  $p = 0.002$ . Representative example in Figure S6D.

**(E)** As in (D), but cells with stable expression of shRNAs against RALA (RALA KD). Mean MFI  $\pm$  SD from biological replicates. Mann Whitney test, ctrl KD vs each sample, \*,  $p = 0.037$ . Representative example in Figure S6E.

**(F)** B cell migration as in Figure 2C. Kruskal Wallis test,  $p = 0.009$ . Mann Whitney test, ctrl KD vs each sample, \*,  $p = 0.05$ .

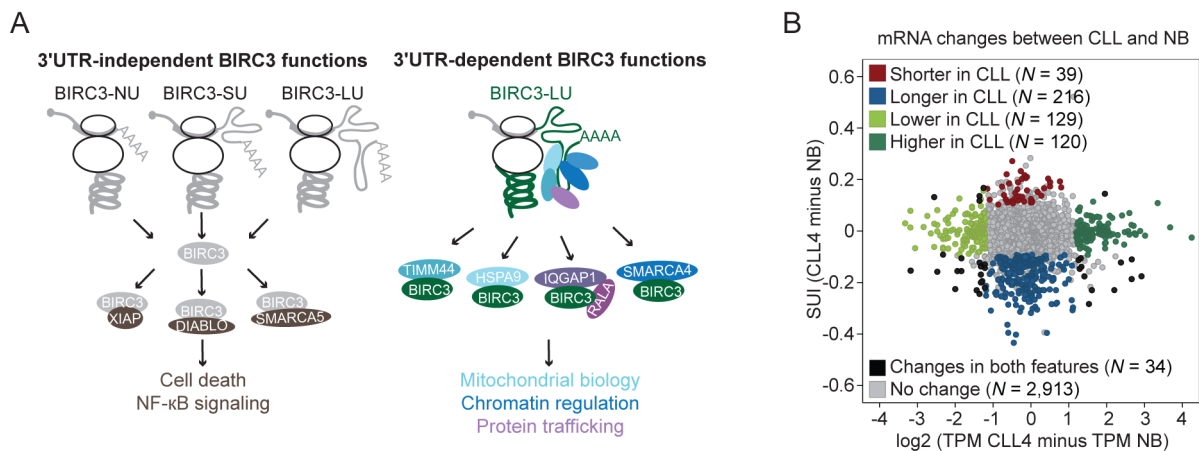


**Figure 7. 3'UTR-dependent protein interactors have the potential to be widespread.**

(A) 3'UTR-independent BIRC3 functions are mediated by 3'UTR-independent protein interactors (brown), including XIAP, DIABLO, and SMARCA5. They can be accomplished when BIRC3 protein is expressed from transcripts containing no regulatory 3'UTR elements (NU), the short 3'UTR (SU) or the long 3'UTR (LU). 3'UTR-dependent BIRC3 roles include the regulation of mitochondrial biology (light blue), chromatin (dark blue), and protein trafficking (purple). These functions are mediated by BIRC3-LU and the 3'UTR-dependent protein interactors including HSPA9, TIMM44, SMARCA4, IQGAP1, and RALA.

(B) Change in mRNA pattern between CLL4 and NB. 3'UTR ratio change is shown on the y-axis and expression change is shown on the x-axis for genes with more than one 3'UTR. Each dot represents an mRNA. Color-coded upon significant difference between the two samples, calculated as in Figure S1A. Red/blue, increased/decreased expression of the short 3'UTR isoform in CLL; dark/light green, higher/lower expression of mRNA in CLL; black, significant change in mRNA levels and change in 3'UTR isoform ratio, and grey indicates no significant change.

## KEY RESOURCES TABLE

REAGENT or RESOURCE	SOURCE	IDENTIFIER
Antibodies		
ACTIN	Sigma-Aldrich	Cat# A4700, RRID:AB_476730
ACTIN	Sigma-Aldrich	Cat# A2066, RRID:AB_476693
GFP	Abcam	Cat# ab13970, RRID:AB_300798
IQGAP1	Sigma-Aldrich	Cat# SAB4200079, RRID:AB_10604111
RALA	Abcam	Cat# ab126627, RRID:AB_11127656
DIABLO	Cell Signaling	Cat# 2954, RRID:AB_2131196
XIAP	Cell Signaling	Cat# 2042, RRID:AB_2214870
SMARCA4	Cell Signaling	Cat# 3508, RRID:AB_2193944
SMARCA5	Cell Signaling	Cat# 38410
HSPA9	Sigma-Aldrich	Cat# SAB4100033, RRID:AB_10743101
TIMM44	Abcam	Cat# ab194829
BAZ1B	Santa Cruz Biotechnology	Cat# sc-514287
ATP5B	Abcam	Cat# ab14730, RRID:AB_301438
VDAC1	Abcam	Cat# ab15895, RRID:AB_2214787
MYC	Sigma-Aldrich	Cat# M4439, RRID:AB_439694
BIRC3 (c-IAP2)	Cell Signaling	Cat# 3130P, RRID:AB_10693298
mCherry	Abcam	Cat# ab125096, RRID:AB_11133266
CXCR4	Santa Cruz Biotechnology	Cat# sc-53534, RRID:AB_782002
ELAVL1 (HuR)	Millipore	Cat# 07-1735, RRID:AB_1977173
STAU1	Proteintech	Cat# 14225-1-AP, RRID:AB_2302744
hnRNPA1	Santa Cruz Biotechnology	Cat# sc-374526, RRID:AB_10991524
hnRNPQ (SYNCRIP)	Sigma-Aldrich	Cat# R5653, RRID:AB_261964
CTR9	Sigma-Aldrich	Cat# SAB1100738, RRID:AB_10013607
SF3B1	Gift from Omar Abdel-Wahab (MSKCC)	N/A
NUDT21	Santa Cruz Biotechnology	Cat# sc-81109, RRID:AB_2153989
FUS	Sigma-Aldrich	Cat# SAB4200478, RRID:AB_2737446
KHSRP	Sigma-Aldrich	Cat# SAB4200566, RRID:AB_2737444
YBX1	Bethyl Laboratories	Cat# A303-231A-M, RRID:AB_2781069
IGF2BP1	Aviva Systems Biology	Cat# ARP40658_P050, RRID:AB_2122664
DDX17	Abcam	Cat# ab24601, RRID:AB_731871
snRNP70	Santa Cruz Biotechnology	Cat# sc-9571, RRID:AB_2193707
hnRNPC	Santa Cruz Biotechnology	Cat# sc-32308, RRID:AB_627731
IgG	Santa Cruz Biotechnology	Cat# sc-2025, RRID:AB_737182
CD27	BD Biosciences	Cat# 555441, RRID:AB_395834
CD47	BD Biosciences	Cat# 561261, RRID:AB_10611734
CD38	BD Biosciences	Cat# 555462, RRID:AB_398599

REAGENT or RESOURCE	SOURCE	IDENTIFIER
CD19	BD Biosciences	Cat# 555415, RRID:AB_398597
CD184 (CXCR4)	BD Biosciences	Cat# 560936, RRID:AB_10563070
anti-mouse IRDye 700	Rockland Immunochemicals	Cat# 610-730-002, RRID:AB_1660934
anti-rabbit IRDye 680	Li-Cor Biosciences	Cat# 926-68073, RRID:AB_10954442
anti-rabbit IRDye 800	Li-Cor Biosciences	Cat# 926-32213, RRID:AB_621848
anti-mouse IRDye 800	Li-Cor Biosciences	Cat# 926-32212, RRID:AB_621847
Bacterial and Virus Strains		
<i>E.coli</i> DH5 alpha	Lab strain	N/A
Biological Samples		
Human CLL cells	Lee, Singh et al., 2018	N/A
Human normal CD5+B cells	Lee, Singh et al., 2018	N/A
Chemicals, Peptides, and Recombinant Proteins		
Tri reagent solution	Invitrogen	Cat# AM9738
Fibronectin	Invitrogen	Cat# 33016-015
Polybrene (hexadimethrine bromide)	Sigma-Aldrich	Cat# H9268
16% Paraformaldehyde, aqueous solution	Fisher scientific	Cat# 50-980-487
Formamide	Sigma-Aldrich	Cat# F7503
Ribonucleoside vanadyl complex	New England Biolabs	Cat# S1402
Dextran sulfate sodium salt	Spectrum Chemical	Cat# DE131
Fludarabine phosphate	Sigma-Aldrich	Cat# F9813
Resazurin	R&D Systems	Cat# AR002
CXCL12	Life technologies	Cat# 10118-HNAE-25
Trypan blue	Sigma-Aldrich	Cat# 93595
CHAPS hydrate	Sigma-Aldrich	Cat# C3023
Na-deoxycholate	Fisher scientific	Cat# BP349-100
Triton X-100	Fisher scientific	Cat# BP151-100
Nonidet P-40	Sigma-Aldrich	Cat# 74385
Sodium chloride	Fisher scientific	Cat# S271-3
Bovine serum albumin (BSA)	Fisher scientific	Cat# BP1605100
Tris base	Fisher scientific	Cat# BP152-1
Q5 High-fidelity DNA polymerase	New England Biolabs	Cat# M0491L
T4 DNA ligase	New England Biolabs	Cat# M0202L
Chloroform	Fisher scientific	Cat# C607-4
Isopropanol	Fisher scientific	Cat# BP26184
Ethanol	Fisher scientific	Cat# BP28184
Methanol	Fisher scientific	Cat# A412-4
SeeBlue® Plus2 pre-stained standard	Invitrogen	Cat# LC5925

REAGENT or RESOURCE	SOURCE	IDENTIFIER
Biotin-UTP	Invitrogen	Cat# AM8450
Phenol	Sigma-Aldrich	Cat# P4682
Critical Commercial Assays		
FastStart universal SYBR green master mix	Roche	Cat# 04913850001
Experimental Models: Cell Lines		
Raji	Gift from Hans-Guido Wendel (MSKCC)	
HEK293T	ATCC	ATCC Cat# CRL-3216, RRID:CVCL_0063
HeLa	Gift from Jonathan Weissman (UCSF)	
Oligonucleotides		
Oligonucleotides for PCR	This paper	Table S4
Oligonucleotides for shRNA cloning	This paper	Table S4
Oligonucleotides for construct cloning	This paper	Table S4
Oligonucleotides for CRISPR guide cloning	This paper	Table S4
Oligonucleotides for Northern blot probe	This paper	Table S4
Recombinant DNA		
pcDNA3.1-GFP-BIRC3-NU	This paper	N/A
pcDNA3.1-GFP-BIRC3-SU	This paper	N/A
pcDNA3.1-GFP-BIRC3-LU	This paper	N/A
pcDNA3.1-GFP	This paper	N/A
pcDNA3.1-GFP- CDR-SU	This paper	N/A
pcDNA3.1-GFP- CDR-LU	This paper	N/A
pcDNA3.1-CXCR4-myc	This paper	N/A
pcDNA3.1-GFP-BIRC3-MS2-SU	This paper	N/A
pcDNA3.1-MCP-mCherry-STAU1	This paper	N/A
pcDNA3.1-MCP-mCherry-HuR	This paper	N/A
pcDNA3.1-MCP-mCherry	This paper	N/A
pSUPERretropuro-shRNA Control	Berkovits and Mayr, 2015	N/A
pSUPERretropuro-shRNA HuR-2	Berkovits and Mayr, 2015	N/A
pSUPERretropuro-shRNA HuR-3	Berkovits and Mayr, 2015	N/A
pSUPERretropuro-shRNA STAU1-1	This paper	N/A
pSUPERretropuro-shRNA STAU1-3	This paper	N/A
pSUPERretropuro-shRNA BIRC3-1	This paper	N/A
pSUPERretropuro-shRNA BIRC3-3	This paper	N/A
pSUPERretropuro-shRNA RalA-2	This paper	N/A
pSUPERretropuro-shRNA RalA-3	This paper	N/A

REAGENT or RESOURCE	SOURCE	IDENTIFIER
pSUPERretropuro-shRNA IQGAP1-1	This paper	N/A
pSUPERretropuro-shRNA IQGAP1-2	This paper	N/A
pCR-Blunt-ARE	This paper	N/A
pCR-Blunt-SU	This paper	N/A
pCR-Blunt-LU	This paper	N/A
pCR-Blunt-LU1	This paper	N/A
pCR-Blunt-antisense SU	This paper	N/A
pCR-Blunt-antisense LU	This paper	N/A
pCR-Blunt-antisense LU1	This paper	N/A
pLKO.1-puro-shRNA IGF2BP1	Sigma-Aldrich	MISSION® shRNA TRCN0000218799, TRCN0000230114
pLKO.1-puro-shRNA Luciferase (control shRNA)	Sigma-Aldrich	MISSION® shRNA SHC007
pX458-BIRC3 guide 3	This paper	N/A
pX458-BIRC3 guide 4	This paper	N/A
Software and Algorithms		
FlowJo	FlowJo	<a href="https://www.flowjo.com">https://www.flowjo.com</a>
Odyssey	LI-COR Biosciences	<a href="https://www.licor.com/bio/products/imaging_systems/odyssey/">https://www.licor.com/bio/products/imaging_systems/odyssey/</a>
MaxQuant	Max Planck Institute of Biochemistry	version 1.5.1.0
Scaffold 4	Proteome Software	version 4.5, <a href="http://www.proteomesoftware.com/products/scaffold/">http://www.proteomesoftware.com/products/scaffold/</a>
MultiGauge	Fuji	
ZEN	ZEISS	<a href="https://www.zeiss.com/microscopy/int/downloads/zen.html">https://www.zeiss.com/microscopy/int/downloads/zen.html</a>
Other		
Lipofectamine 2000	Invitrogen	Cat# 11668019
Trypsin-EDTA (0.05%)	Fisher scientific	Cat# 25300062
Opti-MEM I reduced-serum medium	Invitrogen	Cat# 31985-070
Penicillin-streptomycin solution, 100X	Fisher scientific	Cat# 15070-063
Puromycin	Sigma-Aldrich	Cat# P8833
Protein A/G PLUS-agarose beads	Santa Cruz Biotechnology	Cat# sc-2003
qScript cDNA SuperMix	Quanta Biosciences	Cat# 101414-106
Nucleofactor V kit	Lonza Bioscience	Cat# VCA-1003
Gibson assembly master mix	New England Biolabs	Cat# E2611L
GFP-trap_A beads	Chromotek	Cat# gta-100
2x Laemmli sample buffer	Sigma-Aldrich	Cat# S3401
MES running buffer	Natural Diagnostics	Cat# NP0002
RNase A	Sigma-Aldrich	Cat# R4642
MES running buffer (20X)	Life technologies	Cat# NP0002
MES running buffer (20X)	National Diagnostics	Cat# EC-868



REAGENT or RESOURCE	SOURCE	IDENTIFIER
SILAC culture media	Cambridge Isotope Laboratories	Cat# CNLM-539-H-0.05
SimplyBlue	Invitrogen	Cat# LC6065
Odyssey blocking buffer	Li-Cor Biosciences	Cat# 927-40000
MEGAscript T7	Life technologies	Cat# AM1333
RNaseOUT	Life technologies	Cat# 10777-019
Dynabeads® MyOne™ Streptavidin C1	Life technologies	Cat# 65002
RNase A	Sigma-Aldrich	Cat# R4642
Halt protease inhibitor cocktail	Thermo Fisher Scientific	Cat# 78439
Phosphatase inhibitors 2	Sigma-Aldrich	Cat# P5726
Phosphatase inhibitors 3	Sigma-Aldrich	Cat# P0044

Author Manuscript

Author Manuscript

Author Manuscript

Author Manuscript

TABLE WITH EXAMPLES FOR AUTHOR REFERENCE

REAGENT or RESOURCE	SOURCE	IDENTIFIER
Antibodies		
Rabbit monoclonal anti-Snail	Cell Signaling Technology	Cat#3879S; RRID: AB_2255011
Mouse monoclonal anti-Tubulin (clone DM1A)	Sigma-Aldrich	Cat#T9026; RRID: AB_477593
Rabbit polyclonal anti-BMAL1	This paper	N/A
Bacterial and Virus Strains		
pAAV-hSyn-DIO-hM3D(Gq)-mCherry	Krashes et al., 2011	Addgene AAV5; 44361-AAV5
AAV5-EFla-DIO-hChr2(H134R)-EYFP	Hope Center Viral Vectors Core	N/A
Cowpox virus Brighton Red	BEI Resources	NR-88
Zika-SMGC-1, GENBANK: KX266255	Isolated from patient (Wang et al., 2016)	N/A
<i>Staphylococcus aureus</i>	ATCC	ATCC 29213
<i>Streptococcus pyogenes</i> : M1 serotype strain: strain SF370; MI GAS	ATCC	ATCC 700294
Biological Samples		
Healthy adult BA9 brain tissue	University of Maryland Brain & Tissue Bank: <a href="http://medschool.umaryland.edu/tb/bank/">http://medschool.umaryland.edu/tb/bank/</a>	Cat#UMB1455
Human hippocampal brain blocks	New York Brain Bank	<a href="http://nybb.hs.columbia.edu/">http://nybb.hs.columbia.edu/</a>
Patient-derived xenografts (PDX)	Children's Oncology Group Cell Culture and Xenograft Repository	<a href="http://cogcell.org/">http://cogcell.org/</a>
Chemicals, Peptides, and Recombinant Proteins		
MK-2206 AKT inhibitor	Selleck Chemicals	S1078; CAS: 1032350-13-2
SB-505124	Sigma-Aldrich	S4696; CAS: 694433-59-5 (free base)
Picrotoxin	Sigma-Aldrich	P1675; CAS: 124-87-8
Human TGF- $\beta$	R&D	240-B; GenPept: P01137
Activated S6K1	Millipore	Cat#14-486
GST-BMAL1	Novus	Cat#H00000406-P01
Critical Commercial Assays		
EasyTag EXPRESS 35S Protein Labeling Kit	Perkin-Elmer	NEG772014MC
CaspaseGlo 3/7	Promega	G8090

REAGENT or RESOURCE	SOURCE	IDENTIFIER
TruSeq ChIP Sample Prep Kit	Illumina	IP-202-1012
Deposited Data		
Raw and analyzed data	This paper	GEO: GSE63473
B-RAF RBD (apo) structure	This paper	PDB: 5J17
Human reference genome NCBI build 37, GRCh37	Genome Reference Consortium	<a href="http://www.ncbi.nlm.nih.gov/projects/genome/assembly/grc/human/">http://www.ncbi.nlm.nih.gov/projects/genome/assembly/grc/human/</a>
Nang STILT inference	This paper; Mendelej Data	<a href="http://dx.doi.org/10.17632/wx6s4mj7s8.2">http://dx.doi.org/10.17632/wx6s4mj7s8.2</a>
Affinity-based mass spectrometry performed with 57 genes	This paper; and Mendelej Data	Table S8; <a href="http://dx.doi.org/10.17632/5hyvpspw82.1">http://dx.doi.org/10.17632/5hyvpspw82.1</a>
Experimental Models: Cell Lines		
Hamster: CHO cells	ATCC	CRL-11268
<i>D. melanogaster</i> : Cell line S2: S2-DRSC	Laboratory of Norbert Perrimon	FlyBase: FBtc0000181
Human: Passage 40 H9 ES cells	MSKCC stem cell core facility	N/A
Human: HUES 8 hESC line (NIH approval number NIHhESC-09-0021)	HSCI iPS Core	hES Cell Line: HUES-8
Experimental Models: Organisms/Strains		
<i>C. elegans</i> : Strain BC4011; srl-1(s2500) II; dpy-18(c364) III; unc-46(c177)rol-3(s1040) V.	Caenorhabditis Genetics Center	WB Strain: BC4011; WormBase: WBVar00241916
<i>D. melanogaster</i> : RNAi of Sxl: y[1] sc[*] v[1]; P{TRIP:HMS00609}attP2	Bloomington Drosophila Stock Center	BDSC:34393; FlyBase: FBtp0064874
<i>S. cerevisiae</i> : Strain background: W303	ATCC	ATTC: 208353
Mouse: R6/2; B6CBA-Tg(HDexon1)62Gpb/3J	The Jackson Laboratory	JAX: 006494
Mouse: OXTRf/fl; B6.129(SJL)-Oxtr <sup>tm1.1Wsy/J</sup>	The Jackson Laboratory	RRID: IMSR_JAX:008471
Zebrafish: Tg(Shha:GFP)l10; t10Tg	Neumann and Nüsslein-Volhard, 2000	ZFIN: ZDB-GENO-060207-1
<i>Arabidopsis</i> : 35S::PIF4-YFP, BZR1-CFP	Wang et al., 2012	N/A
<i>Arabidopsis</i> : JYB1021.2; pS24(AT5G58010)::cS24:GFP(G);NOS #1	NASC	NASC ID: N70450
Oligonucleotides		
siRNA targeting sequence: PIP5K I alpha #1: ACACAGUACUCAGUUGAUA	This paper	N/A
Primers for XX, see Table SX	This paper	N/A
Primer: GFP/YFP/CFP Forward: GCACGACTTCTTCAAGTCCGCGCATGCC	This paper	N/A
Morpholino: MO-pax2a GGTCTGCTTTGCAGTGAATATCCAT	Gene Tools	ZFIN: ZDB-MRPHLNO-061106-5
ACTB (hs01060665_g1)	Life Technologies	Cat#4331182

REAGENT or RESOURCE	SOURCE	IDENTIFIER
RNA sequence: hmRNPA1_ligand: UAGGACUUAGGGUUCUCUCUAGGGACUUAGGGUUCUCUCUAGGGGA	This paper	N/A
Recombinant DNA		
pLVX-Tight-Puro (TetOn)	Clontech	Cat#632162
Plasmid: GFP-Nito	This paper	N/A
cDNA GH111110	Drosophila Genomics Resource Center	DGRC:5666; FlyBase:FBcl0130415
AAV2/1-hsyn-GCaMP6- WPRE	Chen et al., 2013	N/A
Mouse raptor: pLKO mouse shRNA 1 raptor	Thoreen et al., 2009	Addgene Plasmid #21339
Software and Algorithms		
Bowtie2	Langmead and Salzberg, 2012	<a href="http://bowtie-bio.sourceforge.net/howtie2/index.shtml">http://bowtie-bio.sourceforge.net/howtie2/index.shtml</a>
Samtools	Li et al., 2009	<a href="http://samtools.sourceforge.net/">http://samtools.sourceforge.net/</a>
Weighted Maximal Information Component Analysis v0.9	Rau et al., 2013	<a href="https://github.com/ChristophRau/wMICA">https://github.com/ChristophRau/wMICA</a>
ICS algorithm	This paper; Mendeley Data	<a href="http://dx.doi.org/10.17632/5hvpvspw82.1">http://dx.doi.org/10.17632/5hvpvspw82.1</a>
Other		
Sequence data, analyses, and resources related to the ultra-deep sequencing of the AML31 tumor, relapse, and matched normal.	This paper	<a href="http://aml31.genome.wustl.edu">http://aml31.genome.wustl.edu</a>
Resource website for the AML31 publication	This paper	<a href="https://github.com/chrisamiller/aml31SuppSite">https://github.com/chrisamiller/aml31SuppSite</a>